OPTIMUM DESIGN OF STIFFENED PANELS WITH SUBSTIFFENERS

David Bushnell,* Fellow, AIAA, Retired
Charles Rankin, Associate Fellow, AIAA
Rhombus Consultants Group, Inc.
Suite B100, 1121 San Antonio Rd., Palo Alto, CA 94303

ABSTRACT

The capability of the computer program PANDA2 to generate minimum-weight designs of stiffened panels and cylindrical shells is enhanced to permit the adding of substiffeners with rectangular cross sections between adjacent major stringers and rings. As a result many new buckling margins exist that govern buckling over various domains and subdomains of the doubly stiffened panel or shell. These generally influence the evolution of the design during optimization cycles. The substiffeners may be stringers and/or rings or may form an isogrid pattern. The effects of local, inter-ring, and general buckling modal imperfections can be accounted for during optimization. Perfect and imperfect cylindrical shells with external T-shaped stringers and T-shaped rings and with and without substringers and subrings and under combined axial compression, external pressure, and in-plane shear are optimized by multiple executions of a "global" optimizer called SUPEROPT. It is found that from the point of view of minimum weight there is little advantage of adding substiffeners. However, with substiffeners present the major stringers and rings are spaced farther apart at the optimum design than is so when there are no substiffeners. The weight of a cylindrical shell with substiffeners is much less sensitive to the spacing of the major T-shaped stringers than is the case for a cylindrical shell without substiffeners. The optimum designs obtained by PANDA2 are evaluated by comparisons with buckling loads obtained from a general-purpose finite element program called STAGS. Predictions from STAGS agree well with those from PANDA2.

INTRODUCTION

Local and overall buckling and optimization of panels can be determined with the PANDA2 [1], POSTOP [2], VICONOPT [3], and PASCO [4] computer programs. These four programs are capable of obtaining optimum designs, and PANDA2, POSTOP, and VICONOPT can do so including the effect of local postbuckling of the panel skin and/or parts of the stringers.

Other contributions to the field of buckling and postbuckling of panels include works by Weaver and his colleagues [5-7], Hilburger, et al[8], Baruch and Singer [9], the creators of the STAGS general purpose program, Almroth, Rankin, Brogan, and Riks [10-12], Arbocz and his colleagues [13-15], Stein [16], Leissa [17], Arnold and Parekh [18], Starnes, Knight, and Rouse [19], Spier [20,21], Khot and Bauld [22,23], Zhang and Matthews [24], Gurdal and his colleagues [25-30], Haftka and his colleagues [30-32], Librescu and his colleagues [33-35], Sridharan and his colleagues [36,37], Myers and Hyer [38], Nemeth [39], and Noor, Starnes, and Peters [40], to identify but a few in a vast literature.

PURPOSE OF THIS PAPER

The purpose of this paper is to report on an enhancement to PANDA2 that permits the optimization of flat and/or cylindrical panels and shells with the "usual" stringers and rings and also with "substiffeners". That is, the skin between the "usual" stringers and rings can be further stiffened by additional members, called "substiffeners" in this work. The substiffeners must be of rectangular cross section. The "usual" stiffeners (stringers and rings) can, as always, have a variety of cross sections, such as rectangular, Tee, Jay, Zee, Hat, Truss-Core, as described in [1]. The new version of PANDA2 is used to find minimum weight designs of cylindrical shells with T-shaped stringers and T-shaped rings and with rectangular substringers and subrings. Figure 1 shows a STAGS model of a piece of a

cylindrical shell with major T-shaped stringers, major T-shaped rings and rectangular (blade) substringers and subrings.

Thermal loading is not included in cases that involve substiffeners. Also, local postbuckling is not permitted in such cases. The objective of this research is to determine if the minimum-weight designs of cylindrical shells with the more complex "double" stiffening scheme are significantly lighter than those optimized with just T-shaped stringers and T-shaped rings.

The substiffeners can also form an isogrid pattern between major axial stiffeners (stringers) and circumferential major stiffeners (rings). If the major stiffeners form an isogrid there cannot be any substiffeners. If there are substiffeners present, there can be no post-local buckling analysis (no "Koiter" analysis,[1,45]). There are no discretized single module models of a segment of panel skin with one substiffener, as with the major stiffeners [1]. In the skin-stringer and skin-ring discretized modules, the substiffeners are smeared out in the manner of Baruch and Singer [9]. Hence, in these discretized module models the new panel "skin" between major stiffeners is the actual panel skin plus smeared substringers and smeared subrings.

Only the panel skin can have substiffeners. As of this writing there can be no substiffeners attached to the webs or outstanding flanges of major stiffeners. The substiffeners cannot be laminated composite. They are modelled as if they were of a single orthotropic material with user-specified E1, E2, G, nu, density, and maximum allowable stress components.

No attempt has yet been made to account properly for THERMAL loading in cases that have substiffeners.

This paper is a summary of a section of the file called .../panda2/doc/panda2.news called "Item no. 600" [1b]. Please see that file for details about input data, output data, and "how to.." directions and suggestions with regard to obtaining optimum designs with the new version of PANDA2. (NOTE: This paper has been updated to account for changes to PANDA2 since panda2.news Item No. 600 was written. However, Item No. 600 has not been updated.)

DESCRIPTION OF PANDA2

PANDA2 is a computer program for the minimum weight design of stiffened, composite, flat or cylindrical, perfect or imperfect panels and shells subjected to multiple sets of combined in-plane loads, normal pressure, edge moments, and temperature. For most configurations the panels can be locally postbuckled. Previous work on PANDA2 is documented in [1]. PANDA2 incorporates the theories of earlier codes PANDA [41] and BOSOR4 [42]. The optimizer used in PANDA2 is called ADS [43,44]. Panels are optimized subject primarily to buckling and stress constraints.

PANDA2 Processors and Types of Analysis

As described in [1], the PANDA2 system consists of several processors, BEGIN, SETUP, DECIDE, MAINSETUP, PANDAOPT, CHOOSEPLOT, CHANGE, STAGSMODEL, STAGSUNIT, etc. The functions of these processors are as follows:

BEGIN	User establishes starting design, material properties, prebuckling and buckling boundary conditions.
SETUP	System sets up BOSOR4-type templates for stiffness and load geometric matrices.
DECIDE	User chooses decision variables and bounds and sets up equality and inequality constraints.
MAINSETUP	User chooses analysis type, loading, and solution strategies.

PANDAOPT	Analysis type is performed (e.g. optimization).
CHOOSEPLOT	User chooses what to plot.
DIPLOT	The system obtains plots (postscript files).
CHANGE	User changes selected variables and constants.
AUTOCHANGE	A new starting design is automatically generated in a random manner.
SUPEROPT	An attempt is made to find a global optimum design.
PANEL	A BOSOR4 input file is generated for inter-ring buckling of panel skin and stringers, with stringers modelled as flexible shell branches.
PANEL2	A BOSOR4 input file is generated for inter-ring buckling of panel skin+smeared stringers with rings modelled as flexible shellbranches.
STAGSMODEL	Input files for STAGS [10-12] are generated (one finite element unit, only stringers are permitted).
STAGSUNIT	Input files for STAGS are generated (multiple shell units, both stringers and rings are permitted).
CLEANPAN	Delete all files except files containing user-provided input data for BEGIN, DECIDE, MAINSETUP, CHANGE, PANEL, PANEL2, STAGSMODEL and STAGSUNIT.

PANDA2 can be run in five modes:
1. optimization
2. simple analysis of a fixed design
3. test simulation
4. design sensitivity
5. load-interaction (Nx,Ny), (Nx,Nxy), (Ny,Nxy)

Types of Buckling Included in PANDA2 Before Substiffeners Added

PANDA2 computes general, inter-ring, and local skin buckling loads and mode shapes. General buckling is buckling in which both stringers (or isogrid stiffeners) and rings participate; panel (inter-ring) buckling is buckling between adjacent rings in which stringers (or isogrid stiffeners) participate but the lines of intersection of ring web roots with the panel skin do not translate; local buckling is buckling of the panel skin between adjacent stringers (or isogrid stiffeners) and rings. PANDA2 includes the following buckling models:

1. A discretized single skin-stringer module. This model is used for local buckling, local postbuckling, and wide column buckling of the panel region between adjacent rings (transverse stiffeners).

2. Simple models for the buckling of the panel skin and stiffener segments of the type described in [41]. Typical buckling modes of the panel skin and stiffeners are shown in Figs. 5 and 6 of [41]. In the panel skin the buckling nodal lines are assumed to be straight, as shown in Fig. 9 of [41]. This type of buckling model is used in some of the software written by Arbocz and Hol [13-15] and by Khot and his colleagues [22,23]. These models are called "PANDA-type (closed form)" in PANDA2 jargon because they are the only ones used in the original PANDA program [41], which was superseded by PANDA2 [1] many years ago. Over the years an elaborate strategy has been developed in order to ensure that for each type of buckling in this PANDA-type category, the most critical (lowest) buckling load factor is not missed. The critical eigenvalue is determined from several searches over various regions in the (m,n,slope) domain, where m is the number of axial halfwaves, n is the number of circumferential halfwaves, and slope is the slope of the buckling nodal lines (non-zero when there is in-plane shear loading and/or

shell wall anisotropy). More details are given in the panda2.news file identified in [1].

For sandwich panels and shells PANDA2 computes load factors for additional types of buckling that only occur for sandwich walls: face sheet wrinkling, buckling over the diameter of a single cell of a honeycomb core, and core crimping [1].

Three additional buckling models were fairly recently added to PANDA2 as described in [1]:

3. Local buckling between adjacent stringers and rings of a cylindrical or flat panel obtained from a Ritz model in which the buckling modal displacement components, u, v, w, are expanded in double trigonometric series. The local region is assumed to be simply supported on all four edges.

4. General buckling of a cylindrical panel in which stringers and rings are treated as discrete beams with undeformable cross sections. Again, the general buckling modal displacement components, u, v, w, are expanded in double trigonometric series. The edges of the domain are assumed to be simply supported and to have discrete stiffeners of half the user-specified modulus. The domain for this model is an M-bay by N-bay subdomain of the entire panel in which M and N are determined by PANDA2.

5. A discretized single module model for a cylindrical panel in which the ring segments and panel skin-with-smeared-stringers are discretized. In this "branched shell" model the cross sections of the rings can deform in the buckling mode, since they are subdivided into finite elements of the type used in BOSOR4[42].

Buckling loads corresponding to a given type of buckling (such as local buckling of the skin between stringers or general buckling) may be computed by more than one model in order to verify results and to provide appropriate knockdown factors to account for anisotropy, inherent unconservativeness in smearing stiffeners, the presence of in-plane shear loading, and variation of in-plane loading within the domain that buckles. The effect of transverse shear deformation (t.s.d.) is accounted for as described in [1].

PANDA2 can optimize imperfect stiffened panels and shells [1]. Imperfections are assumed to be in the shapes of the general, inter-ring, and local buckling modes obtained from the PANDA-type model identified as Item No. 2 above. Imperfections in stiffened panels and shells have two major effects:

a. The imperfect panel or shell bends as soon as any loading is applied. This bending causes significant redistribution of stresses between the panel skin and the various stiffener parts, thus affecting significantly many buckling and stress constraints in the optimization problem.

b. The "effective" curvature of a cylindrical panel or shell depends on the amplitude of the initial imperfection and on the circumferential wavelength of the critical buckling mode of the perfect shell. This "effective" curvature is larger than the nominal radius of curvature because it corresponds to the radius of a typical inward circumferential lobe of the initial and subsequently load-amplified buckling modal imperfection. In PANDA2 this larger local radius of curvature is assumed to be the governing radius in the buckling equations pertaining to the imperfect shell.

Local post buckling analysis

An analysis branch exists in which local post buckling of the panel skin is accounted for [1]. In this branch a constraint condition that prevents stiffener pop-off is introduced into the optimization calculations. The postbuckling theory incorporated into PANDA2 is similar to that formulated by Koiter for panels loaded into the far-postbuckling regime [45].

Stress constraints

In addition to buckling constraints, PANDA2 computes stress constraints including local postbuckling deformations and thermal loading by both curing and applied temperature distributions. For laminated composite walls PANDA2 generates stress constraints corresponding to maximum tension along fibers, maximum compression along fibers,

maximum tension transverse to fibers, maximum compression transverse to fibers, and maximum in-plane shear stress for each different material in a stiffened panel. For isotropic material PANDA2 generates stress constraints based on the von Mises effective stress.

Global optimizer called SUPEROPT introduced into PANDA2

Global optimum designs can be obtained with PANDA2 by means of multiple sequential executions of a processor called SUPEROPT, which is described in more detail in [1]. At intervals during the optimization process new starting designs are automatically generated as follows:

$y(i) = x(i)[1 + dx(i)]$, $i = 1,2,3...$number of decision variables, in which $x(i)$ is the old value of the ith decision variable, $y(i)$ is the new value, and $dx(i)$ is a random number between -0.5 and +1.5 if the decision variable is other than a stiffener spacing and a random number between -1.0 and +1.0 if the decision variable is a stiffener spacing. Stiffener spacings are treated differently from other decision variables because an increase in a stiffener spacing always makes the structure weaker. In order to obtain global optimum designs it is almost always necessary to execute SUPEROPT several times in succession, not just once or twice.

Frequent use of "knockdown" factors in PANDA2

As mentioned in previous PANDA2 literature, in PANDA2 knockdown factors are used often. There are knockdown factors for weakening due to transverse shear deformation (t.s.d.), to compensate for the inherent unconservativeness of smearing stiffeners, to compensate for anisotropic effects and the application of in-plane shear loading, to compensate for initial imperfections, and to compensate for possible truncation error in the double trigonometric series expansions used in the alternative buckling models.

DESCRIPTION OF STAGS

STAGS (STructural Analysis of General Shells) is a finite element code for general-purpose nonlinear analysis of stiffened shell structures of arbitrary shape and complexity. Its capabilities include stress, stability, vibration, and transient analyses with both material and geometric nonlinearities permitted in all analysis types. STAGS includes enhancements, such as a higher order thick shell element, more advanced nonlinear solution strategies, and more comprehensive post-processing features such as a link with STAPL [1b].

Research and development of STAGS by Brogan, Almroth, Rankin, Stanley, Cabiness, Stehlin and others of the Computational Mechanics Department of the Lockheed Palo Alto Research Laboratory has been under continuous sponsorship from U.S. government agencies and internal Lockheed funding for the past 30 years. During this time particular emphasis has been placed on improvement of the capability to solve difficult nonlinear problems such as the prediction of the behavior of axially compressed stiffened panels loaded far into their locally postbuckled states. STAGS has been extensively used worldwide for the evaluation of stiffened panels and shells loaded well into their locally postbuckled states. See [12], for example.

A large rotation algorithm that is independent of the finite element library has been incorporated into STAGS [46]. With this algorithm there is no artificial stiffening due to large rotations. The finite elements in the STAGS library do not store energy under arbitrary rigid-body motion and the first and second variations of the strain energy are consistent. These properties lead to quadratic convergence during Newton iterations.

Solution control in nonlinear problems includes specification of load levels or use of the advanced Riks-Crisfield path parameter [12] that enables traversal of limit points into the post-buckling regime. Two load systems with different histories (Load Sets A and B) can be defined and controlled separately during the solution process. Flexible restart procedures permit switching from one strategy to another during an analysis. This includes shifts from bifurcation buckling to nonlinear collapse analyses and back and shifts from static to transient and transient to static analyses with modified boundary conditions and loading. STAGS provides solutions to the generalized eigenvalue problem for buckling and vibration from a linear or nonlinear stress state.

Quadric surfaces can be modeled with minimal user input as individual substructures called "shell units" in which the analytic geometry is represented exactly. "Shell units" can be connected along edges or internal grid lines with partial or complete compatibility. In this way complex structures can be assembled from relatively simple units. Alternatively, a structure of arbitrary shape can be modeled with use of an "element unit".

Geometric imperfections can be generated automatically in a variety of ways, thereby permitting imperfection-sensitivity studies to be performed. For example, imperfections can be generated by superposition of several buckling modes determined from previous STAGS analyses of a given case.

A variety of material models is available, including both plasticity and creep. STAGS handles isotropic and anisotropic materials, including composites consisting of up to 60 layers of arbitrary orientation. Four plasticity models are available, including isotropic strain hardening, the White Besseling (mechanical sublayer model), kinematic strain hardening, and deformation theory.

Two independent load sets, each composed from simple parts that may be specified with minimal input, define a spatial variation of loading. Any number of point loads, prescribed displacements, line loads, surface tractions, thermal loads, and "live" pressure (hydrostatic pressure which remains normal to the shell surface throughout large deformations) can be combined to make a load set. For transient analysis the user may select from a menu of loading histories, or a general temporal variation may be specified in a user-written subroutine.

Boundary conditions (B.C.) may be imposed either by reference to certain standard conditions or by the use of single- and multi-point constraints. Simple support, symmetry, antisymmetry, clamped, or user-defined B.C. can be defined on a "shell unit" edge. Single-point constraints which allow individual freedoms to be free, fixed, or a prescribed non-zero value may be applied to grid lines and surfaces in "shell units" or "element units". A useful feature for buckling analysis allows these constraints to differ for the prestress and eigenvalue analyses. Langrangian constraint equations containing up to 100 terms may be defined to impose multi-point constraints.

STAGS has a variety of finite elements suitable for the analysis of stiffened plates and shells. Simple four node quadrilateral plate elements with a cubic lateral displacement field (called "410" and "411" elements) are effective and efficient for the prediction of postbuckling thin shell response. A linear (410) or quadratic (411) membrane interpolation can be selected. For thicker shells in which transverse shear deformation is important, STAGS provides the Assumed Natural Strain (ANS) nine node element (called "480" element). A two node beam element compatible with the four node quadrilateral plate element is provided to simulate stiffeners and beam assemblies. Other finite elements included in STAGS are described in the STAGS literature [10-12].

THEORY AND MODIFICATIONS TO PANDA2 TO PERMIT SUBSTIFFENERS

With the introduction of substiffeners between major stiffeners, there are many new buckling constraints introduced into the optimization problem, such as buckling of the panel skin between substiffeners including rolling of the substiffeners, buckling of the panel skin with smeared substringers between adjacent subrings, buckling of the substringers, buckling of the subrings, and buckling from the alternative theory (double trigonometric series expansions) of various "patches" involving segments of the panel skin with discrete substiffeners.

These new constraints are generated in PANDA2 by means of new coding that is analogous to that previously existing for buckling of segments of the major stiffeners and for buckling of sections of the panel skin stiffened by major stiffeners.

In the case of a panel with substiffeners that form an isogrid pattern between adjacent major stringers and rings, a new capability has been implemented with regard to buckling of the triangular portion of panel skin between adjacent isogrid members. Previously, the buckling theory was based on the assumption that the triangular piece of panel skin between adjacent isogrid members was simply supported along its three edges. The contributions of stiffener rolling to the strain energy and work done by prebuckling stiffener resultants during buckling modal rotations were neglected. Now, provided that the stiffeners are of rectangular cross section (as is always the case with substiffeners), these contributions are included. For panels in which the major stiffeners form an isogrid

pattern, if the major stiffeners are of rectangular cross section, their rolling during buckling modal rotations is now included. If the major stiffeners form an isogrid pattern, substiffeners are not allowed.

There are new stress constraints that involve the substiffeners.

EXAMPLE

The numerical results presented here are all derived from an example of an aluminum cylindrical shell, the dimensions, material properties, loading, boundary conditions, and imperfection for which are listed in Table 1. Table 2 lists the names and definitions of all the variables that may or may not be decision variables in optimization problems. Variable No. 2, the stringer base B2(STR), is always equal to one tenth the stringer spacing in this study, and the properties of the wall in the stringer base are the same as those in the wall midway between stringers; there is no stringer faying flange. The width of the ring base, B2(RNG), is always zero in this study.

The new variables pertaining to the substiffeners are called TSUB (thickness), HSUB (height), and BSUB (spacing). In the examples presented here there are always both substringers and subrings.

Table 3 lists the starting design and optimum designs for perfect and imperfect shell with and without substiffeners. One can see from the weights listed that there is little advantage of adding substiffeners from the point of view of weight alone.

RUNSTREAM TO OBTAIN THE "GLOBAL" OPTIMUM DESIGN

The runstream to produce a "global" optimum design is listed in Table 4. The case name is "testax4p". "Global" is in quotes because there is no guarantee that the optimum is truly a global optimum design. The more sets of "superopt/chooseplot/diplot" the user executes, the more likely it is that a truly global optimum design will result. In the "global" optimization in this case, there were four executions of the sequence SUPEROPT /CHOOSEPLOT/DIPLOT.

Each execution of SUPEROPT must be followed by an execution of CHOOSEPLOT because CHOOSEPLOT is where the total number of design iterations gets reset to zero between executions of SUPEROPT. This must always be done before the next execution of SUPEROPT.

Figure 2 shows a plot of the objective function vs design iterations after the first execution of SUPEROPT for the perfect shell with substiffeners. The final optimum design of the perfect shell is listed in Column 3 of Table 3.

RESULTS CORRESPONDING TO THE "GLOBAL" OPTIMUM DESIGN: PERFECT SHELL WITH SUBSTIFFENERS

With substiffeners present there exist many new margins. Table 5 lists the margins corresponding to the optimized perfect cylindrical panel with T-shaped major stringers and T-shaped rings and with rectangular substringers and subrings (case name = "testax4p"). In Table 5 the last six margins correspond to six inequality expressions provided by the PANDA2 user in DECIDE. These six inequality conditions impose the following constraints on the optimum design:

1. The stringer spacing must be at least 3 times the substringer spacing.
2. The ring spacing must be at least 3 times the subring spacing.
3. The substringer height must be less than 10 times the substringer thickness.
4. The subring height must be less than 10 times the subring thickness.
5. The major stringer web height must be less than 20 times the major stringer web thickness.
6. The major ring web height must be less than 20 times the major ring web thickness.

There is one linking constraint: the stringer base width, B2(STR), must equal 0.1 x (stringer spacing B(STR)). In

this case the stringer base has the same thickness and properties as the skin between stringers; there are no faying flanges in any of the cases explored here.

A few of the margins in Table 5 are negative. PANDA2 accepts designs that are "ALMOST FEASIBLE", that is, for which there may be some slightly negative margins, specifically, any margin greater than -0.05.

The optimum dimensions of the perfect shell are listed in Column 3 of Table 3.

The new margins pertaining to substiffeners are listed in Table 6.

In PANDA2 the new margins involving substiffeners are computed in a manner analogous to similar margins involving major stiffeners. For example, Margin 21 in Table 6 is computed from the PANDA-type (closed-form) theory in which the effect of rolling of the substiffeners along the edges of a local region of skin between adjacent substiffeners is included. In PANDA2 models with IQUICK=1 (no discretized skin-stringer module model) and no alternative solution and no substiffeners and major stiffeners with rectangular cross sections, there is an analogous margin:

"buck.(SAND);rolling with local buck.; M=1;N=1;slope=0.2236;FS=1.

computed from the same subroutines.

Margins 22 and 23 in Table 6 are computed from the same subroutines as those for the analogous margins that involve major stiffeners. For example, the "old" margin pertaining to a major stringer (Table 5),

7 1.76E+00 buckling margin stringer Iseg.3 . Local halfwaves=8 .MID.;FS=1.

is computed in SUBROUTINE STFEIG. (In this particular case there is no buckling of ring "Iseg.3" because there exists only tension along the axis of the ring web).

The new margins pertaining to a substringer and subring,

22 -4.04E-04 buckling:simp-support of substring.M=1;FS=1.
23 1.14E+01 buckling:simp-support of subrings N=1;FS=1.

are computed from statements taken from SUBROUTINE STFEIG and inserted in the proper place in SUBROUTINE BUCPAN.

The new margins 24, 25,and 27 in Table 6, computed from the alternative buckling theory described in [1]:

24 -2.86E-02 buckling:simp-support altsoln4 intermajorpatch; FS=0.999
25 3.21E-01 buckling:simp-support altsoln5 skin+edgsubroll; FS=0.999
27 5.78E-02 buckling:simp-support altsoln6 inter-subring ; FS=0.999

are calculated in the same subroutine, ALTSOL, used for computation of the "old" margins (Table 5):

12 1.53E-01 buck.(SAND);simp-support smearsubstf; (0.95*altsol);FS=0.999
13 -3.84E-03 buck.(SAND);simp-support inter-ring; (1.00*altsol);FS=0.999
15 2.35E-03 buck.(SAND);simp-support general buck;(0.85*altsol);FS=0.999

The new alternative buckling models are analogous to the old. The new margin (Table 6),

25 3.21E-01 buckling:simp-support altsoln5 skin+edgsubroll; FS=0.999

is analogous to the "old" one (Table 5),

12 1.53E-01 buck.(SAND);simp-support smearsubstf; (0.95*altsol);FS=0.999

In the new margin (Margin 25) the buckling domain is the panel skin between adjacent substiffeners with rolling of the substiffeners along the edges of the domain included in the model. In the old margin, (Margin 12 in Table 5) the domain is the panel skin + smeared substiffeners between adjacent major stiffeners.

The new margin (Table 6),

27 5.78E-02 buckling:simp-support altsoln6 inter-subring ; FS=0.999
is analogous to the "old" one (Table 5),

13 -3.84E-03 buck.(SAND);simp-support inter-ring; (1.00*altsol);FS=0.999

In the new margin (Margin 27) the buckling domain is the panel skin plus substringers between subrings. A 6-substringer-bay model is used. In the "old" margin (Margin 13) the domain is the panel skin + smeared substiffeners between adjacent major rings. A 6-major-stringer-bay model is now used. (See panda2,news Item No. 603. Previously it was a 3-major-stringer bay model.)

The new margin (Table 6),

24 -2.86E-02 buckling:simp-support altsoln4 intermajorpatch; FS=0.999

is analogous to the "old" one (Table 5),

15 2.35E-03 buck.(SAND);simp-support general buck;(0.85*altsol);FS=0.999

In the new margin (Margin 24) the buckling domain is an N-substringer-bay x M-subring-bay "patch", in which N can be as high as 6 and M can be as high as 5. In the "old" margin (Margin 15) the buckling domain is an N-major-stringer bay x M-major-ring-bay "patch", in which N can be as high as 6 and M can be as high as 5, with substringers and subrings smeared. (See panda2.news Item No. 603 for the recent modification of the way in which the "old" Margin 15 is now computed with a larger "patch" than was previously used. The old "patch" had 3-major-ring bays x 3-major-stringer bays.)

The two new margins pertaining to substiffeners (Table 6),

28 5.77E+00 buck.(SAND);rolling with smear subrng;M=39;N=1;slope=0.01;FS=0.999
29 6.91E-01 buck.(SAND);rolling only of substring;M=20;N=0;slope=0.;FS=1.6

are analogous to the two "old" margins pertaining to major stiffeners (Table 5):

16 5.72E+00 buck.(SAND);rolling with smear rings; M=52;N=1;slope=0.01;FS=0.999
17 6.94E-03 buck.(SAND);rolling only of stringers;M=16;N=0;slope=0.;FS=1.6

The two new margins pertaining to substiffeners (Table 6),

26 2.18E-01 buck.(SAND);rolling with smear substr;M=1;N=2;slope=16.67;FS=0.999
30 8.00E+00 buck.(SAND);rolling only of subrings; M=0;N=4;slope=0.;FS=1.6

are analogous to similar "old" margins pertaining to major stiffeners. However, the "old" margins, although computed, are not recorded as constraints on the design because they are both superceded by the discretized skin-with-smeared-stringers/ring single module model that yields the margin (Table 5),

4 2.53E-02 Inter-ring bucklng, discrete model, n=6 circ.halfwaves;FS=0.999

With the NPRINT index set equal to 2 in the *.OPT file, PANDA2 prints messages
such as the following:

“Inter-ring buckling with smeared stringers and ring rolling is not recorded as a margin because this type of buckling has been superceded by the results from the discretized inter-ring module model, for which inter-ring buckling load factors have been computed in the range from n = 1 to n = 70 circumferential halfwaves. The critical inter-ring-buckling-with-ring-rolling model has 7 circ. half waves, which lies within this range.”

“Ring rolling without participation of the panel skin is not recorded as a margin because this type of buckling has been superceded by the results from the discretized "skin"-ring module model, for which buckling load factors have been computed in the range from n = 1 to n = 70 circ. halfwaves. The critical ring-rolling-without-participation-of-the-panel-skin model has 7 circ. half waves, which lies within this range.”

Please see panda2.news Item No. 463 [1] for more about the discretized module model that involves the panel skin with smeared major stringers and a single discretized major ring cross section and how this model supercedes several buckling constraints that involve major ring rolling. Note that there exists no analogous discretized skin-with-smeared-substringers/subring module model. Therefore, margins such as Margin No. 26 and Margin No. 30 are recorded and not superceded by any other buckling model.

Table 7 lists margins in which the substringers and subrings are smeared in the manner of Baruch and Singer [9].

Margins 1-3 in Table 7:

1 2.53E-02 Local buckling from discrete model-1.,M=2 axial halfwaves;FS=0.99
2 2.23E-01 Bending-torsion buckling; M=2 ;FS=0.999
3 3.24E-01 (m=2 lateral-torsional buckling load factor)/(FS)-1;FS=0.999

are from the discretized "skin"-major-stringer single module model. In Margin 1 the term "local" means "local buckling of the "skin" between major stringers. In the presence of substiffeners, what used to be called the panel skin is now the panel skin-with-smeared-substiffeners. Margins 2 and 3 are computed from the same discretized single module model with smeared substiffeners.

With substiffeners present there exist buckling modes more local than that corresponding to Margin 1. For example, the margin,

21 4.60E-01 buck.(SAND);rolling with skin buckl.; M=1;N=1;slope=0.1939;FS=0.999

(Table 6) involves local buckling of the panel skin between adjacent substiffeners, with rolling of the substiffeners included in the model.

Margins 4 and 13 in Table 7,

4 2.53E-02 Inter-ring bucklng, discrete model, n=6 circ.halfwaves;FS=0.999
13 -3.84E-03 buck.(SAND);simp-support inter-ring; (1.00*altsol);FS=0.999

are computed with substiffeners smeared and major stringers smeared.

Margin 12 in Table 7,

12 1.53E-01 buck.(SAND);simp-support smearsubstf; (0.95*altsol);FS=0.999

used to be called "buck.(SAND);simp-support local buckling; (0.95*altsol)". It is generated from the same alternative buckling theory (double trigonometric series expansion) as before when there existed only skin between adjacent stringers and rings. Now the domain between adjacent major stringers and rings includes smeared substiffeners.

Margins 14 and 15 in Table 7,

14 -2.02E-02 buck.(SAND);simp-support general buck;M=6;N=0;slope=0.4637;FS=.999

15 2.35E-03 buck.(SAND);simp-support general buck;(0.85*altsol);FS=0.999

are derived from two different models of general instability, a closed form PANDA-type model in which all stiffeners (major and sub) are smeared out (Margin 14) and an alternative (double trig series expansion) model in which the substiffeners are smeared out and the major stiffeners are treated as discrete beams in a 6-major stringer bay by 5-major-ring-bay "patch" (Margin 15).

Margin 16 in Table 7,

16 5.72E+00 buck.(SAND);rolling with smear rings; M=52;N=1;slope=0.01;FS=0.999

is generated from a model in which the substiffeners as well as the major rings are smeared out and the major stringers are treated as discrete beams that run along the two generators at the straight edges of the long, narrow domain that includes the entire length of shell between two adjacent major stringers.

GENERATING AN OPTIMUM DESIGN THAT CAN BE ANALYZED WITH STAGS

It is important to evaluate the optimum design obtained by PANDA2 by use of a general-purpose finite element program operating on the same design. The general-purpose finite element program STAGS [10-12] was used. The PANDA2 processor STAGSUNIT [1] had to be modified to work for panels with substiffeners [1b].

In order to generate a PANDA2 model that, via STAGSUNIT, produces suitable input files, *.bin and *.inp, for STAGS, it is necessary first to find an optimum design with PANDA2 in which there are integral numbers of major stiffeners over the entire domain of the STAGS model and integral numbers of substiffeners between adjacent major stiffeners. This is done by the following steps:

1. Use the PANDA2 processor called CHANGE to reset the variables, B(STR), B2(STR), B(RNG) BSUB(substringer), BSUB(subrings) so that there are integral numbers of each kind of stiffener in the appropriate domains. Choose values that are close to those found in the optimum designs listed in Table 3. (See Table 8 for appropriate values of the stiffener spacings for STAGS models).

2. Use the PANDA2 processor called DECIDE. The stiffener spacings B(STR), B2(STR), B(RNG) BSUB(substringer), BSUB(subrings), should no longer be decision variables, and the therefore inappropriate inequality constraints,

a. The stringer spacing must be at least 3 times the substringer spacing.
b. The ring spacing must be at least 3 times the subring spacing.

should be eliminated.

3. Execute SUPEROPT/CHOOSEPLOT/DIPLOT at least once to find a new "global" optimum design for which there are integral numbers of major stiffeners and substiffeners in the appropriate domains.

4. Execute PANDAOPT once more for a fixed design: the optimum design.

New optimum designs suitable for analysis by STAGS are listed in Table 8. The margins corresponding to the perfect shell with substiffeners (second column in Table 8) are listed in Table 9.

CREATION OF STAGS MODELS

STAGS models, such as that shown in Fig. 1, are generated via the PANDA2 processor called STAGSUNIT. The purpose of STAGSUNIT is to generate the two input files, *.bin and *.inp, for the STAGS general purpose finite element program. In this example "*" stands for the case name, "testax4p". Typical input data files for STAGSUNIT are listed in several tables in [1b].

As described in [1], the processor STAGSUNIT is written in such a way that "patches" of various portions of a complete panel or shell can be analyzed with STAGS. The correct prebuckled state of a perfect panel is preserved independently of the size of the "patch" to be included in the STAGS model. The minimum size "patch" must contain at least one major stiffener spacing in each direction, and major stringers are always included along the two straight edges of the "patch". There may or may not be rings running along the two curved edges of the "patch", depending on input to STAGSUNIT provided by the user of PANDA2. Stiffeners that run along the four boundaries of the "patch" have half the stiffness of those that lie within the "patch". Figure 1 shows a STAGS "patch" model that includes only three bays between major stringers (four major stringers) and one bay between two major rings.

Substiffeners always lie within the patch. There must always be integral numbers of uniformly spaced substiffeners (substringers and/or subrings) between adjacent major stiffeners. The substiffeners that are closest to the major stiffeners are one half a substiffener spacing away from the major stiffeners. Substringers and subrings never occur along coordinate lines where there exist major stringers and/or major rings. As of this writing STAGSUNIT cannot handle isogrid stiffening or substiffening.

The STAGS models are constructed by the PANDA2 processor STAGSUNIT in such a way that all stiffeners (major and sub) are connected only to the panel skin. That is, where stiffeners intersect they simply pass through eachother with no constraints between them along their lines of intersection. This is a conservative model with respect to buckling.

There can be gaps between the roots of the stiffeners and the reference surface of the panel skin. For example, if the reference surface of the panel skin is the middle surface, there are gaps equal to half the skin thickness. The user can elect to have what in STAGS jargon are called "fasteners" that relate the nodal displacement components on the skin reference surface to those at the root of a stiffener web. The STAGS model shown in Fig. 1 has fasteners. They can barely be seen as tiny black dots at nodal points along the roots of all the stiffeners.

Several examples of input data for the PANDA2 processor, STAGSUNIT, are given in [1b]. Detailed instructions on running STAGSUNIT followed by running STAGS are also listed there.

RESULTS FROM STAGS

The execution of STAGS produces a number of files. The user must inspect the *.out1 and *.out2 files if the STAGS run bombs. The user must inspect the *.out2 file if the run finishes in a normal fashion.

Table 10 lists the most important part of the testax4p.out2 file generated from the successful STAGS run to which Fig. 3 corresponds: a three-axial-bay by nine- circumferential-bay "patch" in which all of the major stiffeners and substiffeners are modelled as shell units and in which the "480" STAGS finite element is used throughout the STAGS model. The middle surface is used as the reference surface of the cylindrical skin and there exist fasteners that connect this middle surface to the roots of the stiffeners.

The buckling modes corresponding to the eigenvalues (buckling load factors) listed in Table 10 are all mixtures of the types corresponding to the following margins from PANDA2 (Table 9):

```
 1  1.24E-01 Local buckling from discrete model-1.,M=2   axial halfwaves;FS=0.99
 2  3.38E-01 Bending-torsion buckling; M=2  ;FS=0.999
 3  4.50E-01 (m=2   lateral-torsional buckling load factor)/(FS)-1;FS=0.999
 4  1.03E-02 Inter-ring bucklng, discrete model, n=6   circ.halfwaves;FS=0.999
13 -3.76E-03 buck.(SAND);simp-support inter-ring;  (1.00*altsol);FS=0.999
17 -2.58E-02 buck.(SAND);rolling only of stringers;M=14;N=0;slope=0.;FS=1.6
24 -4.18E-02 buckling:simp-support altsoln4  intermajorpatch; FS=0.999
```

The numbers listed under "TYPES OF BUCKLING" in Table 10 correspond to the PANDA2 margins from Table 9 and repeated just above.

According to PANDA2, the three types of buckling

1 1.24E-01 Local buckling from discrete model-1.,M=2 axial halfwaves;FS=0.99
2 3.38E-01 Bending-torsion buckling; M=2 ;FS=0.999
3 4.50E-01 (m=2 lateral-torsional buckling load factor)/(FS)-1;FS=0.999

are not critical. In contrast, these three modes play a prominant role in the STAGS model of buckling. In PANDA2 the domain used for these three types of buckling includes only the axial dimension between adjacent major rings. Therefore, the string "M=2" means "two axial halfwaves between major rings". In the STAGS model the axial wavelength of the "bending-torsion" buckling or "lateral-torsional" buckling (sidesway of the major stringers) is not restricted to the distance between adjacent major rings because the stiffeners are allowed to deform relative to eachother where they intersect. The PANDA2 model that leads to the margin,

17 -2.58E-02 buck.(SAND);rolling only of stringers;M=14;N=0;slope=0.;FS=1.6

also allows the stringers to deform relative to the major rings because the domain is the entire axial length of the panel. Therefore, the string "M=14" means "14 axial halfwaves over the entire axial length of the panel". The inclusion of this type of buckling prevents PANDA2 from yielding an unconservative design in this case because the buckling domain is longer than one major ring spacing.

Figure 3 shows the buckling mode from STAGS corresponding to the lowest eigenvalue (buckling load factor), 0.97738. Figure 4 shows the "same" STAGS model and buckling mode except that the STAGS 410 finite element is used for the panel skin and the major stiffeners and the STAGS 210 finite element is used for the substiffeners. If any stiffeners (major or sub) are modelled as beams (210 element), then the user has no choice: the STAGS 410 element MUST be used for all shell units since this element is compatible with the STAGS 210 beam element.

Figure 5 shows the fundamental buckling mode from the same model that produced Figure 3 except that the substiffeners are smeared out in the manner of Baruch and Singer [9]. The buckling modes from STAGS are similar to those corresponding to the STAGS models in which the substiffeners are treated as shell units except that there is little evidence of the type of buckling from PANDA2's margin 24: "intermajorpatch".

GENERAL BUCKLING MODE(S) FROM STAGS

Of particular interest is the determination of the general buckling load factor according to STAGS. In this case one must include the entire cylindrical shell in the STAGS model. Because of the presence of uniform in-plane shear loading, Nxy, (Table 1) there are no planes of symmetry. In the STAGS model of the entire shell the substiffeners are smeared out and the major stiffeners are treated as shell units. The STAGS "480" finite element is used throughout. The outer surface of the panel skin is used as the reference surface and there are no fasteners in this particular model.

In order to find the lowest long-wavelength general buckling mode in this case it is necessary to make several STAGS runs, each successive run with a slightly higher initial eigenvalue "shift". This has to be done because there are many "inter-ring" buckling modes that have eigenvalues (buckling load factors) that bracket the lowest eigenvalue corresponding to the general buckling mode. "Inter-ring" is in quotation marks here because most of these short-wavelength modes involve significant in-plane bending of the major rings, as will be seen later. This places them in the "general buckling" category. Three STAGS runs were required in this case to obtain the lowest long-wavelength general buckling mode (Mode 19).

There are results from two sets of three runs each listed in Table 600.24 of [1b]. The first set of three runs corresponds to a model in which the outer surface of the shell skin is used as a reference surface and there are no fasteners. The second set of three runs corresponds to a model in which the middle surface of the shell skin is used as a reference surface and there are fasteners. The effect of this difference in modeling is minor: The buckling load factors from the model with fasteners are from one to two per cent lower than those without fasteners.

The general buckling load factor, 1.0511, for the "no fasteners" model, corresponds to the 19th eigenvalue. This

general buckling mode has three circumferential waves. The general buckling load factor, 1.04201, for the "fasteners" model, also corresponds to the 19th eigenvalue for that model and also has three circumferential waves.

The buckling mode corresponding to the lowest eigenvalue, 1.022198E+00, is shown in Fig. 6 and the buckling mode for the lowest eigenvalue corresponding to long-wavelength general instability, 1.051100E+00, is shown in Fig. 7. Both of these modes are for the STAGS model with no fasteners. The modes for the STAGS model with fasteners, corresponding to the first eigenvalue, 1.008428, and to the 19^{th} eigenvalue, 1.042010, are essentially the same.

All of the other eigenvalues correspond approximately to "inter-ring" buckling modes similar to that in Fig. 6. In these relatively short wavelength buckling modes the axes of the stringers deform and the rings primarily twist. However, for most of the rings the axes of the rings also deform, as shown in Fig. 8. Figure 8 is produced by elimination of all the shell units except the two shell units that correspond to the web and outstanding flange of the fourth ring from the left end of the model shown in Fig. 6. In Fig. 8 the buckling modal deformations for the same mode (Mode No. 1) as that shown in Fig. 6 are plotted to the same scale as is shown in Fig. 6. Because there is significant bending in the plane of this and in the planes of the other rings, these "inter-ring" modes may also be considered to have significant components of general buckling: a short-wavelength general buckling mode similar in type to that shown in Figs. 21, 26, 27, 29 of the paper, "Additional buckling solutions in PANDA2" [1].

For a complete (360 degrees) cylindrical shell the converged eigenvalues (buckling load factors) occur in pairs. This is typical in STAGS models of complete (360-degree) cylindrical shells. The buckling mode corresponding to each eigenvalue in a pair is the same except that one mode in the pair is rotated around the shell circumference relative to the other.

RESULTS FROM STAGS MODELS OF THE COMPLETE CYLINDRICAL SHELL WITH ALL STIFFENERS (MAJOR AND SUB) SMEARED

STAGS produces the results listed in Table 11. The critical buckling mode is shown in Fig. 9 and the buckling mode corresponding to the third eigenvalue, 1.371375, is shown in Figs. 10 and 11. The axisymmetric buckling load factor, 1.371375, is not far above the critical buckling load factor, 1.288339, which corresponds to a general buckling mode with three circumferential waves, essentially the same buckling mode as that shown in Fig. 7.

A similar STAGS model was run with use of the "410" finite element rather than the "480" finite element. For that model, the same nodal point density leads to a prediction of general buckling at a load factor (eigenvalue) of 1.340773, reasonably close to the 1.288339 obtained from the model with use of the 480 finite element. The order of the n=2 and n=0 modes is reversed compared to that for the model in which the STAGS "480" finite element was used (Table 11).

Although the critical general buckling mode according to STAGS has long wavelengths (one halfwave in the axial direction and three full waves over the entire circumference), a model in which all stiffeners are smeared produces a prediction that is unacceptably unconservative (Table 11). Compare the STAGS buckling load factor, 1.288339, from the smeared stiffener model with the STAGS buckling load factor from the model in which the substiffeners are smeared but the major stiffeners are modelled as shell units and fasteners are included: lowest eigenvalue = 1.04201. The model in which all stiffeners are smeared is unconservative by about 24 per cent.

With use of the "410" finite element rather than the "480" finite element in the STAGS model, the unconservativeness of the smeared model: general buckling load factors = 1.340773E+00 vs 1.042010E+00, is even more pronounced. The conclusion is that even though the general buckling mode in Fig. 7 appears to be smooth, it does not seem to be good practice to smear the major stiffeners for optimized shells. Models with smeared stiffeners may well lead to unacceptably unconservative designs.

COMMENTS ON DIFFERENCES IN BUCKLING MODES FROM STAGS AND PANDA2 FOR THE PERFECT SHELL

STAGS is a general-purpose finite element program. Therefore, the buckling modes obtained from STAGS do not necessarily have to fall into a classification such as "general" or "inter-ring" or "local" or "stiffener rolling without participation of the panel skin", etc. For example, a buckling mode from STAGS may be a combination of "general" and "inter-ring". The buckling load factors listed in Table 10 correspond to buckling modes of this "mixed" type. Also, the buckling mode shown in Figs. 6 and 8 is a mixture of general and inter-ring buckling.

What may be termed a "general buckling" mode from STAGS for descriptive purposes is not always a "pure" general buckling mode. The AIAA Paper 2002-1408 [1] shows examples of "pure" and "not so pure" general buckling modes. Figure 25 of that paper shows a "pure" general buckling mode; Figure 24 shows a "somewhat impure" general buckling mode; and Figure 23 shows a "very impure" general buckling mode. The "impure" general buckling modes have differing degrees of short-wavelength deformation superposed on what is basically a general buckling mode. (Incidentally, Figures 20-22 of AIAA Paper 2002-1408 show an "inter-ring" buckling mode similar in nature to the "inter-ring" modes in the present case; there is considerable deformation of at least one ring in its plane, as displayed in Fig. 22 of that paper, making the mode a combination of "inter-ring" buckling and "general buckling".)

The classifications of "general", "inter-ring", "local", etc. ARE meaningful in the PANDA2 "universe", however. PANDA2 arrives at reasonable optimum designs with reasonable computer execution times through the use of many different simplified models for the prediction of buckling and stress. In applying PANDA2, one expects that the appropriate combination of these simplified models will lead to reliable preliminary optimum designs that are not too conservative and for which all the "holes have been plugged", that is, there are not any critical modes of failure that have been overlooked. Over the many years that PANDA2 has been evolving, many such "holes" have been discovered and eliminated. (See the file, ..panda2/doc/panda2.news [1]).

Table 600.30 in [1b] lists results from PANDA2 computations for the types of buckling that are seen to occur in the STAGS models of the complete (360-degree) cylindrical shell to which the results shown in Figs. 6-11 correspond. Results from ten different buckling models are listed there, including three models of inter-ring buckling, two models of general buckling, and five models of stiffener buckling. Several comments, "<--NOTE...", and several paragraphs of comments have been added to the standard PANDA2 output listed in Table 600.30 in [1b] in order to help give the reader a physical "feel" for what is going on. The information given in that table, which is too long to include in this paper, should be absorbed by any researcher interested in using PANDA2 and interested in understanding how it tries to solve difficult shell problems reasonably accurately through the use of many different approximate models. (NOTE: panda2.news ITEM No. 600 was written during February and early March, 2005. Since then there have been many changes in PANDA2, documented in panda2.news items 601 – 621. This paper has been updated accordingly. However, panda2.news ITEM No. 600 was not updated. Therefore some of the results listed there are not what one would obtain currently. The overall conclusions and the basic philosophy and approach to solving the various buckling problems remains unchanged. Therefore panda2.news ITEM No. 600 remains a useful teaching tool.

The critical STAGS buckling mode for short-wavelength "general" buckling is shown in Fig. 6 and the critical STAGS buckling mode for long-wavelength general buckling is shown in Fig. 7. As seen from Fig. 8 the short-wavelength "general" buckling mode has five circumferential waves around the 360-degree circumference of the cylindrical shell. The long-wavelength general buckling mode has three circumferential waves.

PANDA2 uses two models for general instability, to which the following two margins, taken from Table 9, correspond:

14 -3.66E-02 buck.(SAND);simp-support general buck;M=6;N=0;slope=0.473;FS=0.999
15 6.26E-04 buck.(SAND);simp-support general buck;(0.85*altsol);FS=0.999

The first margin, Margin No. 14, is computed from the closed-form PANDA-type model [41]. In that model all

stiffeners are smeared out and transverse shear deformation (t.s.d.) is neglected. PANDA2 makes an elaborate search over (m,n,slope) = (MWAVEX,NWAVEX,SLOPEX) space for the critical (lowest) buckling load factor, EIGMNC, in which MWAVEX = number of axial halfwaves over the entire shell, NWAVEX = number of circumferential halfwaves over 180 degrees of circumference (the "width" of the panel = pi x r), and SLOPEX = the slope of the buckling nodal lines, non-zero in this case because of the presence of in-plane shear loading, Nxy = 20000 lb. The search over (m,n,slope) space must be thorough because there often are multiple minima of buckling load factor vs (m,n,slope). The following lines are typical PANDA2 output giving the results of this thorough search:

EIGMNC=	1.52E+00	1.52E+00	1.69E+00	1.93E+00	1.69E+00	1.52E+00	1.48E+00
SLOPEX=	6.81E-01	6.81E-01	1.00E-02	1.32E-01	0.00E+00	6.81E-01	4.73E-01
MWAVEX=	1	1	7	6	7	1	6
NWAVEX=	3	3	2	4	2	3	0

In this particular case there are at least four minima in (m,n,slope) space, corresponding to (m,n) = (1,3), (7,2), (6,4), and (6,0) and various nodal line slopes. [Question: Why do we write, "at least four minima", instead of, "four minima"? Answer: For given (m,n) there are often two minmima over the practical range of nodal line slope]. PANDA2 chooses the smallest EIGMNC as the critical buckling load factor and mode shape for general buckling from the closed-form PANDA-type theory [41].

Notice that in this particular case the general buckling load factors corresponding to the buckling modes (m,n.slope) = (1,3,0.681) and (6,0,0.473) are fairly close: 1.52 and 1.48, respectively. The (1,3,0.681) buckling mode is similar to the STAGS mode from the smeared stiffener model shown in Fig. 9. The (6,0,0.473) buckling mode is similar to the STAGS mode from the smeared stiffener model shown in Figs. 10 and 11 (axisymmetric mode).

PANDA2 "knocks down" the most critical buckling load factor from PANDA-type theory as follows:

Buckling load factor before t.s.d.= 1.4820E+00 After t.s.d.= 1.4019E+00
Buckling load factor BEFORE knockdown for smeared stringers= 1.4019E+00
Buckling load factor AFTER knockdown for smeared stringers = 1.3147E+00

General buckling load factor before and after knockdown:

EIGGEN(before modification by 2 factors below) = 1.3147E+00
Knockdown factor from modal imperfection(s) = 9.4144E-01
Knockdown factor for smearing rings on cyl. Shell = 7.7761E-01

Final buckling load factor from closed-form PANDA theory = 9.6249E-01

Note that there is a knockdown factor for modal imperfection(s) even though in this particular example the shell is perfect. Why? Because the ratio, (ARBOCZ/PANDA2) is equal to 0.94144. The ratio, (ARBOCZ/PANDA2) is the ratio of buckling loads from ARBOCZ theory [13] to PANDA-type (closed form) theory [41] for general buckling of a perfect cylindrical shell.

After knockdown, EIGENVALUE = 9.6249E-01. This buckling load factor should be compared to those predicted from STAGS, given in Fig. 6 (pcr = 1.0222) and Fig. 7 (pcr = 1.0511). The EIGENVALUE, 9.6249E-01, is the buckling load factor from which Margin No. 14 in Table 9 is derived:

margin = (buckling load factor)/(factor of safety) - 1.0
= 0.96249/0.999 -1.0 = -3.66E-02.

The most critical general buckling mode from PANDA2 probably would have corresponded to the (m,n) = (1,3) mode if the knockdown factor for smearing rings, which depends on the number of circumferential waves in the buckling mode, had been applied before PANDA2 decided which mode was the most critical. Then the long-wavelength general buckling mode shape from STAGS (Fig. 7) would have agreed with that from PANDA2. However, this is not the way PANDA2 works, and it is not feasible to change the order of computations in PANDA2.

The other model of general instability in PANDA2 is the so-called "alternative buckling theory" in which the buckling load factor is computed from a double trigonometric series expansion of the buckling modal displacements over a "patch" of the cylindrical shell [1]. This is the theory from which Margin No. 15 in Table 9 is computed. The mode shape corresponding to the buckling load factor derived from this alternative buckling theory resembles an inter-ring buckling mode, although there are components of buckling modal displacements that give rise to some in-plane bending of the rings. In the alternative theory model for general buckling the substiffeners are smeared.

The short-wavelength STAGS buckling mode shown in Figs. 6 and 8 seems to be a combination of inter-ring buckling of the type covered by PANDA2 in Margin No. 4 of Table 9,

4 1.03E-02 Inter-ring bucklng, discrete model, n=6 circ.halfwaves;FS=0.999

and general buckling from the alternative theory covered by Margin No. 15 of Table 9,

15 6.26E-04 buck.(SAND);simp-support general buck;(0.85*altsol);FS=0.999

Thus, by the use of several approximate models that cover the same or similar buckling phenomena, PANDA2 produces margins that guide the design toward an optimum similar to one that might be produced by STAGS if STAGS were used in an optimization context.

STAGS MODEL FOR LOCAL BUCKLING

It is best to determine local buckling behavior from a rather small "patch". In this case the STAGS "patch" includes only one bay between major rings, with a major ring at each end of the "patch", and three bays between major stringers, with a major stringer running along each straight edge (generator) of the "patch". Hence, the "patch" is 37.5 inches long in the axial direction and 43.836 inches long in the circumferential direction. The major stiffeners that run along the four boundaries of the "patch" have half the stiffnesses of those that lie within the "patch". As mentioned previously, all of the substiffeners lie within the "patch". Figures 1, 12, 13, and 14 show the STAGS "patch" model suitable for a local buckling survey. The STAGS 480 finite element is used, the reference surface is the middle surface of the panel skin, and there are fasteners connecting this reference surface to the roots of all of the stiffeners. The fasteners are seen as tiny black dots at the stiffener roots shown in Figs. 1, 12, 13, and 14.

The purpose of the STAGS model with use of a small "patch" is to compare predictions with the various models that PANDA2 uses for the many types of buckling that can be classified as "local" in this case. The buckling margins from Subcase 1 in Table 9 that seem to apply best in this context are as follows:

1 1.24E-01 Local buckling from discrete model-1.,M=2 axial halfwaves;FS=0.99
2 3.38E-01 Bending-torsion buckling; M=2 ;FS=0.999
3 4.50E-01 (m=2 lateral-torsional buckling load factor)/(FS)-1;FS=0.999
7 1.45E+00 buckling margin stringer Iseg.3 . Local halfwaves=8 .MID.;FS=1.
8 -3.99E-03 buckling margin stringer Iseg.4 . Local halfwaves=8 .MID.;FS=1.
9 4.64E-01 buckling stringer Isegs.3+4 together.M=9 ;C=0. ;MID.;FS=1.4
10 7.63E-02 buckling stringer Iseg 4 as beam on foundation. M=198;MID.;FS=3.
11 1.43E+01 buckling ring Iseg 4 as beam on foundation. M=140;MID.;FS=3.
12 2.95E-01 buck.(SAND);simp-support smearsubstf; (0.95*altsol);FS=0.999
13 -3.76E-03 buck.(SAND);simp-support inter-ring; (1.00*altsol);FS=0.999
17 -2.58E-02 buck.(SAND);rolling only of stringers;M=14;N=0;slope=0.;FS=1.6
18 7.89E-01 buck.(SAND);hiwave roll. of stringers;M=84;N=0;slope=0.;FS=1.2
19 1.43E+00 buck.(SAND); STRINGERS: web buckling;M=9;N=1;slope=0.;FS=1.
20 1.51E+01 buck.(SAND); RINGS: web buckling;M=2;N=1;slope=0.;FS=1.
21 4.86E-01 buck.(SAND);rolling with skin buckl.; M=1;N=1;slope=0.1978;FS=0.999
22 6.44E-03 buckling:simp-support of substring.M=1;FS=1.
23 1.41E+01 buckling:simp-support of subrings N=1;FS=1.
24 -4.18E-02 buckling:simp-support altsoln4 intermajorpatch; FS=0.999

25 3.18E-01 buckling:simp-support altsoln5 skin+edgsubroll; FS=0.999
26 1.21E-01 buck.(SAND);rolling with smear substr;M=1;N=2;slope=20.;FS=0.999
27 1.16E-02 buckling:simp-support altsoln6 inter-subring ; FS=0.999

Many buckling modes were generated via five STAGS runs, each successive run made with use of a slightly higher eigenvalue "shift" in the STAGS input file, testax4p.bin. Table 600.32 of [1b] lists the abridged testax4p.out2 files from each of the five STAGS executions. Figure 1 shows the buckling mode and eigenvalue (buckling load factor) corresponding to the critical (lowest) buckling load, 0.98903. Figures 12 - 14 show selected higher buckling modes, modes that display especially well some of the idealized buckling modes of the type computed by PANDA2 and listed above and in Table 9.

DESCRIPTION OF PANDA2 MODELS OF VARIOUS MODES OF LOCAL BUCKLING

Table 600.33 in [1b] is analogous to Table 600.30 in [1b]. Table 600.33 in [1b] lists output from PANDA2 corresponding to thirteen models of local buckling that PANDA2 includes as design constraints. The local buckling modes from STAGS listed in Table 600.32 of [1b] are combinations of the simplified buckling models listed in Table 600.33 of [1b] This table is too long to include here. As with Table 600.30 in [1b] its information should be absorbed by researchers interested in using PANDA2.

Figures 1 and 12 - 14 show selected buckling modes from the STAGS "patch" model. Figure 1 shows buckling of the panel skin and substiffeners together with some deformation of the major stringers, a mode covered by PANDA2 margins 1 and 24. Figure 12 shows mainly buckling between subrings with subring rolling and substringers participating in the buckling mode. This type of buckling is covered by PANDA2 margins 26 and 27. Figure 13 shows mainly rolling of the stringers, a mode covered by PANDA2 Margin No. 17. Figure 14 displays a combination of local buckling modes covered by PANDA2 margins 21, 22, and 25.

OPTIMUM DESIGN INCLUDING INITIAL BUCKLING MODAL IMPERFECTION

A general buckling modal imperfection with amplitude Wimpg2 equal to 1.0 inch is assumed. The case is the same as before except it is called "testax4" instead of "testax4p" (the "p" in testax4p is for "perfect").

The testax4.BEG and testax4.DEC files, listed in [1b], are the same as those for testax4p. The new testax4.OPT file is listed in Table 600.35 of [1b]. There are two load cases, the first with a positive general buckling modal imperfection (+1.0 inch) and the second with a negative general buckling modal imperfection (-1.0 inch). The optimum design is listed in Column 4 of Table 3. This optimum design was obtained via the runstream listed in Table 4.

In order to obtain a new (close) optimum design that is suitable for analysis by STAGS, we must ensure that there are integral numbers of equally spaced major stiffeners over the entire shell and integral numbers of equally spaced substiffeners between adjacent major stiffeners, just as we did with the perfect shell (testax4p). The final optimum design suitable for analysis by STAGS is listed in the third column of Table 8. As before, this optimum design is obtained with the use of two load cases: the first with an initial general buckling modal imperfection with amplitude Wimpg2 = +1.0 inch and the second with imperfection amplitude Wimpg2 = -1.0 inch. The margins corresponding to Load Case 1, Subcase 1 are listed in Table 12.

In the STAGS runs the imperfection is not present. If we wish to compare the behavior of the newly optimized shell with the imperfection neglected, we must execute PANDAOPT again for the same design, this time with the imperfection amplitude set equal to zero. This was done and the new margins for Load Case 1, Subcase 1 are listed in Table 13.

PANDA2 generates two estimates of general buckling, one from a PANDA-type (closed form) theory (Margin No. 16 in Load Set 1, Subcase 1 in Table 12 and Margin No. 14 in Load Set 1, Subcase 1 in Table 13) and the other from the alternative, double trigonometric series expansion, theory (Margin No. 17 in Load Set 1, Subcase 1 in Table 12 and Margin No. 15 in Load Set 1, Subcase 1 in Table 13). These margins are given by

a. Including the initial general buckling modal imperfection (Table 12, Wimp=1.0 inch):

16 -1.35E-02 buck.(SAND);simp-support general buck;M=1;N=2;slope=25.;FS=0.999
17 4.01E-02 buck.(SAND);simp-support general buck;(0.85*altsol);FS=0.999

b.Neglecting the initial buckling modal imperfection (Table 13, Wimp=0.0):

14 1.96E-01 buck.(SAND);simp-support general buck;M=1;N=2;slope=25.;FS=0.999
15 4.78E-01 buck.(SAND);simp-support general buck;(0.85*altsol);FS=0.999

Note that the initial general buckling modal imperfection has a much smaller influence on the buckling margin derived from the PANDA-type (closed form) theory (Margin 16 with the imperfection and Margin 14 without the imperfection) than on the buckling margin derived from the alternative (double trig series expansion) theory (Margin 17 with the imperfection and Margin 15 without the imperfection). This difference in behavior is explained in Table 600.42 in [1b]. In the PANDA-type (closed form) model the redistribution of stress from stiffeners to skin during prebuckling bending of the imperfect shell has no influence on the predicted buckling load or mode because all stiffeners are smeared out in the PANDA-type model. Hence, this simplified theory makes use only of the overall applied stress resultants which are the same whether there is or is not an initial imperfection. In the alternative theory, in which the major stiffeners are treated as discrete beams and only the substiffeners are smeared out, the redistribution of stress from major stiffeners to skin-with-smeared-substiffeners during prebuckling bending of the imperfect shell does have an influence on the predicted buckling load and mode shape. This influence is apparent from the output from PANDA2 listed in Table 600.42 in [1b] and from a comparison of Margin No. 17 with Margin No. 15 listed just above.

RESULTS FROM STAGS FOR THE CASE testax4 WITH IMPERFECTION ABSENT

The STAGS model includes the entire shell. The major stiffeners are treated as shell units, the substiffeners are smeared, and the STAGS "480" finite element is used. The outer surface of the panel skin is the reference surface and there are no fasteners connecting this reference surface to the roots of the major stiffener webs.

Figure 15 shows the general instability buckling mode from the STAGS model with only the substiffeners smeared, and Fig. 16 shows the same mode with all stiffeners (major and sub) smeared. Note that smearing the major stiffeners raises the buckling load factor from 1.4468 to 1.8058, about 25 per cent. Even though the critical general buckling mode is smooth and has long wavelengths a model in which the major stiffeners are smeared yields an unacceptably unconservative prediction for general buckling.

With neglect of the initial general buckling modal imperfection, PANDA2 obtains the following general buckling margin (from Table 13):
14 1.96E-01 buck.(SAND);simp-support general buck;M=1;N=2;slope=20.;FS=0.999
(buckling load factor = (buckling margin + 1.0)*(factor of safety, FS).
 buckling load factor = (0.196 + 1.0)*(0.999) = 1.1948)
The PANDA2 prediction is about 17 per cent conservative compared to the STAGS prediction, and PANDA2 predicts buckling with two rather than three circumferential waves. The PANDA2 buckling load factor for general buckling is computed as follows:

EIGMNC=	2.07E+00	2.07E+00	2.10E+00	3.91E+00	2.10E+00	2.07E+00	1.00E+17
SLOPEX=	4.00E-02	4.00E-02	0.00E+00	1.32E-01	0.00E+00	4.00E-02	2.31E+00
MWAVEX=	1	1	1	6	1	1	1
NWAVEX=	2	2	2	5	2	2	0

Buckling load factor before t.s.d.= 2.0713E+00 After t.s.d.= 1.9586E+00
Buckling load factor BEFORE knockdown for smeared stringers= 1.9586E+00
Buckling load factor AFTER knockdown for smeared stringers= 1.8367E+00

General buckling load factor before and after knockdown:
EIGGEN(before modification by 2 factors below) = 1.8367E+00
Knockdown factor from modal imperfection(s) = 8.9150E-01
Knockdown factor for smearing rings on cyl. shell = 7.2989E-01

14 1.19515E+00 buckling load factor simp-support general buck;M=1;N=2;slope=20.

A second STAGS model includes three major ring bays and nine major stringer bays for the case called testax4. All the stiffeners, major as well as sub, are treated as shell units, there are fasteners, and the STAGS "480" finite element is used. This is the same type of model as that used for the optimized perfect shell and shown in Fig. 3.

Figure 17 shows the second buckling mode from the STAGS 3 x 9 bay "patch" model. The second mode rather than the first is shown because the modal deformations show up better in the plot. (The first two eigenvalues are practically identical).

A third STAGS model includes one major ring bay and three major stringer bays for the case called testax4. All the stiffeners, major as well as sub, are treated as shell units, there are fasteners, and the STAGS "480" finite element is used. This is the same type of model as that used for the optimized perfect shell and shown in Figs. 1 and 12-14.

Figures 18 and 19 show buckling modes from the STAGS 1 x 3 bay "patch". The buckling mode corresponding to the lowest eigenvalue, 1.2757, is displayed in Fig. 18, and the buckling mode corresponding to the third eigenvalue, 1.3099, is displayed in Fig. 19.

Figure 18 is a combination of the PANDA2 modes from Table 13,

2 2.21E-01 Long-axial-wave bending-torsion buckling; M=2 ;FS=0.999
17 7.94E-02 buck.(SAND);rolling only of stringers;M=12;N=0;slope=0.;FS=1.6

and Fig. 19 is a combination of the PANDA2 modes from Table 13,

8 1.35E-01 buckling margin stringer Iseg.4 . Local halfwaves=8 .MID.;FS=1.
9 7.26E-01 buckling stringer Isegs.3+4 together.M=8 ;C=0. ;MID.;FS=1.4
12 2.71E-01 buck.(SAND);simp-support smearsubstf; (0.95*altsol);FS=0.999
13 7.45E-02 buck.(SAND);simp-support inter-ring; (1.00*altsol);FS=0.999
22 3.87E-02 buckling:simp-support of substring.M=1;FS=1.
24 1.94E-01 buckling:simp-support altsoln4 intermajorpatch; FS=0.999
26 6.03E-01 buck.(SAND);rolling with smear substr;M=1;N=1;slope=14.29;FS=0.999
27 5.63E-01 buckling:simp-support altsoln6 inter-subring ; FS=0.999
25 4.39E-01 buckling:simp-support altsoln5 skin+edgsubroll; FS=0.999
27 3.49E-01 buckling:simp-support altsoln6 inter-subring ; FS=0.999

RESULTS FOR A SIMILAR STIFFENED SHELL WITHOUT SUBSTIFFENERS

The name of the case for the externally T-stiffened cylindrical shell with the same overall dimensions (Table 1) but without any substiffeners is "testax3". It is of interest to optimize this shell and to compare the optimized weights of perfect and imperfect shells without substiffeners with the optimized weights of perfect and imperfect shells with substiffeners.

There are two inequality conditions in testax3.DEC (Table 600.51 in [1b] not present in the preceeding cases, testax4p and testax4, in which substiffeners are present. The first of these two new inequality constraints requires that the width of the flange of the T-ring be less than the ring spacing. The second new inequality constraint requires that the spacing of the T-stringers be less than five times the spacing of the T-rings. After several preliminary optimizations it became clear that these two additional inequality conditions were required for the following reasons:

1. to prevent impossible designs in which the rings become so closely spaced or their outstanding flanges so wide that the outstanding flanges overlap.

2. to prevent "bombs" from SUPEROPT caused by a requirement that for an IQUICK = 0 type of analysis the stringers must be closer together than a distance equal to five times the ring spacing. This condition is built into PANDA2; the user has no choice. When it is violated SUPEROPT bombs because PANDA2 demands a change of model from IQUICK = 0 to IQUICK = 1 and then exits from the mainprocessor, not completing the rest of the SUPEROPT run.

The difficulties leading to the need for these two new inequality constraints arise because, without any substiffeners present, optimum designs tend to correspond to configurations in which the T-shaped stiffeners are close together.

The optimum design of the perfect shell is listed in the fifth column of Table 3. This optimum results from the runstream listed in Table 4. The fourth column of Table 8 lists the optimum design of the perfect shell without substiffeners that is suitable for analysis by STAGS (integral numbers of equally spaced stringers and rings over the entire shell). The corresponding margins for Load case 1, Subcase 1 are listed in Table 14.

COMPARISON OF THE OPTIMIZED DESIGNS OF THE PERFECT SHELLS WITH AND WITHOUT SUBSTIFFENERS

The weights of the optimized perfect shells with and without substiffeners are listed in columns 3 and 5, respectively, of Table 3. It is disappointing that the difference in optimized weights of the perfect cylindrical shells with and without substiffeners is insignificant. For the optimized perfect cylindrical shell with substiffeners the weight of the shell skin plus the weight of the substiffeners is close to the weight of the shell skin in the optimized cylindrical shell without substiffeners. The weights of the major stringers and the weights of the major rings are approximately the same in the two cases. It is not worthwhile including substiffeners just to save weight.

However, substiffeners may be considered if it is important that the number of major stringers be minimized. The spacing of the major stringers in the optimized cylindrical shell with substiffeners is given in Table 3 by B(STR) = 14.775 inches. In contrast, the spacing of the stringers in the optimized cylindrical shell without substiffeners is B(STR) = 5.2141 inches.

There is a somewhat less dramatic effect on the spacing of the major rings:

39.157 B(RNG):major ring spacing perfect shell WITH substiffeners
22.208 B(RNG):major ring spacing perfect shell WITHOUT substiffeners.

Optimized designs of the perfect, externally T-stiffened cylindrical shells with and without substiffeners were determined for a range of spacing of the major stringers. The results are shown in Fig. 20, generated via a plotting routine "plotps" written by W. D. Bushnell [1]. From Fig. 20 one can see that the weight of the optimized cylindrical shells without substiffeners is much more sensitive to spacing of the major stringers than is the case for the optimized cylindrical shells with substiffeners. This seems to be the only advantage of adding substiffeners of rectangular cross section to the panel skin.

Other loadings, such as external hydrostatic compression (Nx = p*r/2; Ny = p*r) and load combinations with more in-plane shear Nxy, were investigated with the same conclusion: there is very little if any advantage of adding substiffeners of rectangular cross section in order to decrease minimum weight as long as the stringer spacing is permitted to vary widely during optimization cycles. Also, the advantage of adding substiffeners of rectangular cross section disappears if stresses become critical.

Different conclusions might be drawn if the substiffeners have other than rectangular cross section. PANDA2 is not yet capable of handling substiffeners with non-rectangular cross sections. Also, it may be that adding substiffeners to other parts of the structure than the panel skin would be advantageous. Perhaps lighter-weight shells could be made if substiffeners were added to webs and outstanding flanges of the major stiffeners. There are no plans at this time to expand PANDA2's capability to handle any of these new geometries.

RESULTS FROM STAGS FOR THE OPTIMIZED PERFECT SHELL WITHOUT SUBSTIFFENERS

The fourth column of Table 8 lists the optimum design of the perfect shell without substiffeners that is suitable for analysis by STAGS (integral numbers of equally spaced stringers and rings over the entire shell). The corresponding margins for Load case 1, Subcase 1 are listed in Table 14.

The PANDA2 processor STAGSUNIT was used to generate a STAGS model corresponds to a "patch" that includes three ring bays and nine stringer bays. The middle surface of the panel skin is the reference surface and there are fasteners that connect the roots of the stiffener webs to this reference surface (tiny black dots in Fig. 21). The critical buckling mode for the "patch" is displayed in Fig. 21. This mode is similar in character to the buckling modes shown for a similar "patch" of the optimized perfect shell with substiffeners in Figs. 3-5.

An endview plot of the same buckling mode appears in Fig. 22, which shows clearly that there are five circumferential halfwaves in the nine-stringer-bay "patch". This patch spans 47.124 inches of shell circumference [9 x (B(STR)=5.236 in Col. 4 of Table 8) = 47.124 inches]. The 47.124-inch-wide "patch" represents 1/13.333th of the 360-degree shell circumference. Hence, the same buckling pattern over the entire circumference would have 66.667 half waves over 360 degrees or about 33 halfwaves over 180 degrees. This mode is in very good agreement with that predicted by PANDA2 for inter-ring buckling from the PANDA-type (closed form) analyis (PANDA2 buckling mode type 5 listed in Table 14):

5 1.57E-01 Inter-ring bucklng, discrete model, n=32 circ.halfwaves;FS=0.999

STAGSUNIT was used to generate a STAGS model of the optimized, perfect, complete cylindrical shell. The T-shaped stringers and T-shaped rings are modeled as shell units, and the STAGS "480" finite element is used. The outer surface of the shell skin is used as the reference surface and there are no fasteners. At the optimum design of the perfect shell the T-shaped stringers are very closely spaced; there are 120 of them over the entire (360-degree) circumference. There are 15 T-rings over the 300-inch length of the cylindrical shell. Since each T-shaped stringer consists of two shell units and each T-shaped ring consists of two shell units, there are 1 + (2 x 120) + (2 x 15) = 271 shell units in this very large STAGS model. This STAGS model has about 580000 degrees of freedom.

The STAGS model predicts general buckling in a mode with three circumferential waves at a load factor of 1.060638. This general buckling mode corresponds to the 25th eigenvalue. Figure 23 shows the general buckling mode from STAGS. All the other eigenvalues correspond to inter-ring buckling in which the stringers bend. The lowest eigenvalue (buckling load factor) is 1.0512. The corresponding buckling mode is displayed in Fig. 24. It was difficult to find the one general buckling mode hidden like a needle in a haystack among a thicket of short-wavelength buckling modes of the type shown in Fig. 24. (See ACKNOWLEDGMENTS).

With the stringers and rings smeared out and with use of the 480 finite element, the lowest eigenvalue corresponds to general buckling at a load factor of 1.170279, an increase of about 10 per cent over that for the more accurate model: 1.060638. The general buckling mode is the same as that found for the STAGS model in which all stiffener parts were modelled as shell units. With use of the 410 finite element in the smeared stiffener model the lowest eigenvalue increases from that computed with use of the 480 element, eigenvalue=1.170279, to eigenvalue=1.194869.

Note that for this shell without substiffeners, in which the T-shaped stringers and T-shaped rings are more closely spaced than is the case for the optimized shell with substringers, the degree of unconservativeness caused by smearing the major stiffeners is significantly less than for the optimized shell with substringers. In those cases (testax4p for the perfect shell and testax4 for the imperfect shell) smearing the major stiffeners raises the buckling load factor for general instability from 1.0511 to 1.2883 for the optimized PERFECT shell with substiffeners and from 1.4468 to 1. 8058 for the optimized IMPERFECT shell with substiffeners.

Notice in Table 14 that the margin corresponding to general buckling from the closed-form PANDA-type theory [41],

13 -3.53E-02 buck.(SAND);simp-support general buck;M=8;N=0;slope=0.335;FS=0.999

shows that the critical buckling mode from PANDA2 has (m,n) = (MWAVEX,NWAVEX) = (8,0) halfwaves in the (axial, circumferential) directions. This is similar to the critical general buckling mode from PANDA2 discussed at some length for the optimized perfect shell with substiffeners. In that case PANDA2 predicts the critical (m,n) = (6,0). As with the optimized shell with substiffeners, in the present case the critical long-wavelength general buckling mode predicted by STAGS for the shell without substiffeners, shown in Fig. 23, is very different from that predicted by PANDA2. According to STAGS the critical long-wavelength buckling mode has one axial halfwave and three circumferential waves.

For the optimized perfect shell without substiffeners PANDA2 yields the following results from the exhaustive search over (m,n,slope) = (MWAVEX,NWAVEX,SLOPEX) space:

EIGMNC=	1.30E+00	1.30E+00	1.27E+00	1.54E+00	1.35E+00	1.30E+00	1.00E+17
SLOPEX=	2.77E+00	2.77E+00	3.35E-01	1.32E-01	0.00E+00	2.77E+00	0.00E+00
MWAVEX=	1	1	8	8	9	1	0
NWAVEX=	3	3	0	4	1	3	0

Notice that the buckling load factors, EIGMNC for (m,n,slope) = (1,3,2.77) and (8,0,0.335) are close: EIGMNC = 1.30 and 1.27, respectively. As mentioned in this context previously, if the knockdown factor for smearing rings had been applied before PANDA2 chooses which mode is critical, PANDA2's prediction of buckling mode shape probably would have agreed with that from STAGS. What is important in this computation of buckling is not the buckling mode shapes but the buckling load factors. They are what control the evolution of the design of the perfect shell during optimization cycles.

RESULTS FOR THE OPTIMIZED IMPERFECT SHELL WITHOUT SUBSTIFFENERS

The optimum design resulting from the runstream listed in Table 4 is listed in the last column in Table 3. The optimum design suitable for analysis by STAGS is listed in the last column in Table 8. As with the imperfect shells with substiffeners, the optimum designs without substiffeners were obtained with application of two load cases:

1. Load Case 1: general buckling modal imperfection amplitude, Wimpg2 = +1.0 inch,
2. Load Case 2: general buckling modal imperfection amplitude, Wimpg2 = -1.0 inch.

The margins corresponding to the optimized design suitable for analysis by STAGS are listed in Tables 15 and 16.

COMPARISON OF OPTIMUM DESIGNS OF IMPERFECT EXTERNALLY T-STIFFENED CYLINDRICAL SHELLS WITH AND WITHOUT SUBSTIFFENERS

As is the case for the perfect optimized shells with substiffeners, a comparison of the optimum weights of the imperfect shells with and without substiffeners reveals that the weight saving by introduction of substiffeners is small (6.2 percent from Table 3 and 5.6 percent from Table 8). (Compare weights in columns 4 and 6 of Table 3 and columns 3 and 5 of Table 8).

As with the optimized perfect shells with and without substiffeners, the major stiffeners weigh about the same amount for the optimized imperfect shells with and without substiffeners. The panel skin for the optimized imperfect cylindrical shell without substiffeners weighs about 8.3 per cent more than the skin plus substiffeners of the optimized cylindrical shell with substiffeners.

The spacing of the major stringers in the optimized imperfect cylindrical shell with substiffeners is given in Table 3 as B(STR) = 11.424 inches. In contrast, the spacing of the major stringers in the optimized imperfect cylindrical shell without substiffeners is given by B(STR) = 5.760 inches. Hence, as with the perfect shells, the presence of substiffeners of rectangular cross section permits the major stringers to be spaced at much wider intervals around the cylindrical shell.

There is a much less dramatic effect on the spacing of the major rings:

42.874 B(RNG):major ring spacing, imperfect shell with substiffeners
28.291 B(RNG):major ring spacing, imperfect shell without substiffeners.

Probably the spacing of the major rings would be influenced more by the presence of substiffening for loading by hydrostatic compression, in which the hoop compression is twice the axial compression, in contrast to the cases explored here, in which the axial compression is five times the hoop compression.

RESULTS FROM STAGS FOR THE DESIGN LISTED IN COLUMN 5 OF TABLE 8 (testax3)

The linear buckling analysis by STAGS for a three-ring-bay by nine-stringer-bay "patch" of the optimized shell yields a buckling load factor of 1.3252 (initial imperfection not present in the STAGS model). With the amplitude of the general buckling modal imperfection set equal to zero, PANDA2 obtains the following margins (among other margins) for that design:

2 3.86E-01 Long-axial-wavw bending-torsion buckling; M=1; FS=0.999
4 4.53E-01 (m=1 lateral-torsional buckling load factor)/FS-1; FS=0.999
5 7.76E-01 Inter-ring bucklng, discrete model, n=33 circ.halfwaves;FS=0.999
13 1.72E-01 buck.(SAND);simp-support inter-ring; (1.00*altsol);FS=0.999
17 1.44E-01 buck.(SAND);rolling only of stringers;M=12;N=0;slope=0.;FS=1.6

The circumferential width of the "patch" in the STAGS model is 51.8796 inches, which corresponds to 1/12.111th of the 360-degree circumference of the shell. The lowest buckling load factor from STAGS, 1.3252, is associated with a buckling mode that has five circumferential halfwaves over the 51.8796-inch width of the "patch". This mode translates into 5 x 12.111/2 = 30 full circumferential waves over the entire 360-degree circumference of the shell. This mode is in agreement with the buckling mode associated with the 5th margin in the PANDA2 model:
5 7.76E-01 Inter-ring bucklng, discrete model, n=33 circ.halfwaves;FS=0.999

which has 33 circumferential halfwaves over 180 degrees of the circumference of the shell. The three buckling margins from PANDA2, Margins 2, 4, 5, 13, and 17, cover the type of buckling observed in the STAGS model.

PANELS WITH SUBSTIFFENERS THAT FORM AN ISOGRID

The "substiffener" capability in PANDA2 was extended to include panels with axial and circumferential major stiffeners and a skin that may be reinforced by substiffeners of rectangular cross section that form an isogrid pattern between adjacent major stringers and rings. Results from optimizations of perfect and imperfect cylindrical shells with external T-shaped stringers and external T-shaped rings and with external subisogrid stiffening are given in [1b]. Also presented in [1b] is the improvement to the theory for local buckling of the triangular piece of panel skin between adjacent isogrid or subisogrid members. The improved theory includes the contribution of the isogrid members to the total potential energy, provided that the cross section of the isogrid members is rectangular.

As with the cases involving axial and circumferential substiffeners, for the various loadings investigated it was found that there is no weight saving from introduction of subisogrid stiffening. The optimized weight of the perfect shell with an external subisogrid is 17392 lb, which is greater than the optimized weight of the perfect shell with no substiffeners (16846 lb) and greater than the optimized weight of the perfect shell with axial and circumferential substiffeners (16712 lb). The optimized weight of the imperfect shell with an external subisogrid is 21560 lb, which is less than the optimized weight of the imperfect shell without substiffeners (21620 lb) and greater than the optimized weight of the perfect shell with axial and circumferential substiffeners (20560 lb).

With subisogrid stiffening the optimum designs have major stiffeners spaced farther apart than for the optimum designs without any substiffeners, although the difference in spacing between the case with substiffeners and that without is less pronounced than for the cases involving axial and circumferential substiffeners.

OTHER SUBSTIFFENING CONFIGURATIONS

Cases involving substringers and subrings on opposite sides of the panel skin and involving internal substringers and internal subrings combined with external major T-shaped stringers and external T-shaped major rings were explored. Some results are presented in [1b], especially for the case of a perfect cylindrical shell with external major stringers and major rings and internal substringers and subrings. The optimzed weight of this perfect cylindrical shell is 16612 lb, slightly less than the 16712 lb for the optimized
weight of the perfect cylindrical shell with external substringers and subrings.

NONLINEAR COLLAPSE

In the paper, AIAA 2002-1408 [1], nonlinear collapse is computed for a ring and stringer stiffened cylindrical shell with general and local buckling modal imperfections. Figures 27 and 28 of that paper show the results from such an analysis. Collapse occurs because both the general and local imperfections grow as the load is increased. Unfortunately, it was not possible to perform a similar analysis in the effort leading to the present paper for the following reasons:

1. The entire shell must be included in the model because there are no planes of symmetry due to the presence of in-plane shear loading, Nxy = 20000 lb/in.

2. In the example of the optimized imperfect shell without substiffeners, the T-shaped stiffeners are so close together that a converged finite element model would contain too many degrees of freedom to capture the local component of collapse, which is seen as small dimples in Fig. 27 of AIAA Paper 2002-1408 [1]. It was barely possible to compute the general buckling mode from linear theory for a similar model (Fig. 23). A nonlinear collapse analysis requires far more computer resources. Also, as Fig. 24 demonstrates, the very large STAGS model is probably not large enough to capture accurately either inter-ring buckling or local buckling between adjacent stringers and rings.

3. In the example of the optimized imperfect shell with substiffeners one might well conduct a nonlinear collapse analysis in a model in which the substiffeners are smeared, such as that shown in Fig. 15. However, an analysis of this type would simply be a repeat of the type of study that produced Figs. 27 and 28 in AIAA Paper 2002-1408. It would not reveal the effect of prebuckling bending of the globally imperfect shell on the local buckling behavior of panel skin and substiffeners, such as that displayed in Figs 1, 12, and 14 of the present work. A model of the complete cylindrical shell that would capture the complex local behavior of shell skin and substiffeners would require far more degrees of freedom (d.o.f.) than the approximately 580000 d.o.f. model needed to predict the general buckling mode shown in Fig. 23.

CONCLUSIONS

Adding substiffeners of rectangular cross section between major stiffeners does not lead to significantly lower optimum weights. However, with substiffeners present the optimum weights correspond to configurations in which the major stiffeners are spaced farther apart than is the case for optimized cylindrical shells without substiffeners.

ACKNOWLEDGMENTS

The author (D. Bushnell) is most grateful for the help of Dr. Frank Weiler, a friend and colleague at Lockheed Martin in Palo Alto, California. Dr. Weiler frequently helped Bushnell whenever any problems arose in connection with executing STAGS on various computers at the Lockheed Martin Advanced Technology Center. Dr. Weiler ran and reran and reran and reran the 580000-degree-of-freedom STAGS model generated by the file listed in Table 600.62 of [1b] and shown in Figs 23 and 24. Several reruns at different "eigenvalue shifts" were required in order to capture the lowest general buckling mode, which was buried like a needle in a haystack among a thicket of local

buckling modes. Each run required about 40 minutes on the computer. (Dr. Weiler had to use a special computer with enhanced memory and disk capacities. That computer, a Pentium 4 desktop with two gigabytes of memory, was available to him only.) The author, David Bushnell, also very much appreciates the help of his son, Bill Bushnell, in obtaining proper formats for Tables 2 – 16.

REFERENCES

[1] D. Bushnell, "PANDA2-Program for minimum weight design of stiffened, composite, locally buckled panels", Computers and Structures, Vol. 25 (1987) pp. 469-605. See also: "Optimization of composite, stiffened, imperfect panels under combined loads for service in the postbuckling regime", Computer Methods in Applied Mechanics and Engineering, Vol. 103, pp 43-114, 1993; "Recent enhancements to PANDA2" 37th AIAA SDM Conference, April 1996; "Approximate method for the optimum design of ring and stringer stiffened cylindrical panels and shells with local, inter-ring, and general buckling modal imperfections", Computers and Structures, Vol. 59, No. 3, 489-527, 1996; "Optimum design via PANDA2 of composite sandwich panels with honeycomb or foam cores", AIAA Paper 97-1142, AIAA 38th SDM Conference, April 1997; "Additional buckling solutions in PANDA2", AIAA 40th SDM Conference, p 302-345, April 1999; "Minimum-weight design of a stiffened panel via PANDA2 and evaluation of the optimized panel via STAGS", Computers and Structures, Vol. 50, 569-602 (1994); "Optimization of perfect and imperfect ring and stringer stiffened cylindrical shells with PANDA2 and evaluation of the optimum designs with STAGS", AIAA Paper 2002-1408, pp 1562-1613, Proceedings of the 43rd AIAA SDM Meeting, April, 2002;

[1b] D. Bushnell, .../panda2/doc/panda2.news, a continually updated file distributed with PANDA2 that contains a log of all significant modifications to PANDA2 from 1987 on. In particular, see ITEM No. 600 in that file, which contains more details about the "substiffener" project..

[2] J. N. Dickson, S. B. Biggers, and J. T. S. Wang, "Preliminary design procedure for composite panels with open-section stiffeners loaded in the post-buckling range," in: Advances in Composite Materials, A. R. Bunsell, et al,editors, Pergamon Press Ltd., Oxford, England, 1980, pp 812-825. Also see, J. N. Dickson and S. B. Biggers, "POSTOP: Postbuckled open-stiffened optimum panels, theory and capability", NASA Langley Research Center, Hampton, Va., NASA Contractor Report from NASA Contract NAS1 -15949, May 1982.

[3] Butler, R. and Williams, F. W., "Optimuam design features of VICONOPT, an exact buckling program for prismatic assemblies of anisotropic plates," AIAA Paper 90-1068-CP, Proceedings 31st AIAA/ASME Structures, Structural Dynamics, and Materials Meeting, pp 1289-1299. Also see Williams, F. W., Kennedy, D., Anderson, M.S., "Analysis features of VICONOPT, an exact buckling and vibration program for prismatic assemblies of anisotropic plates,", AIAA Paper 90-0970-CP, Proceedings 31st AIAA/ASME Structures, Structural Dynamics, and Materials Meeting, pp 920-929

[4] M. S. Anderson and W. J. Stroud, "General panel sizing computer code and its application to composite structural panels," AIAA Journal, 17, (1979) pp. 892-897. Also see W. J. Stroud and M. S. Anderson, "PASCO: Structural panel analysis and sizing code, capability and analytical foundations," NASA TM-80181, NASA Langley Research Center, Hampton, Va., 1981. Also see W. J. Stroud, W. H. Greene and M. S. Anderson, "Buckling loads of stiffened panels subjected to combined longitudinal compression and shear: Results obtained with PASCO, EAL, and STAGS computer programs," NASA TP 2215, Nasa Langley Research Center, Hampton, Va., January 1984.

[5] Wong, K. F. W. and Weaver, P. M., "Approximate solution for the compression buckling of fully-anisotropic cylindrical shells", 45th AIAA Structures, Structural Dynamics & Materials Conference, April 2004, Palm Springs, California

[6] Weaver, P. M., "On optimisation of long anisotropic flat plates subject to shear buckling loads", 45th AIAA SDM Conference, April 2004

[7] Diaconu, C. G. and Weaver, P. M., "Approximate solution and optimum design for postbuckling of infinite laminated composite plates subjected to compression loading", 45th AIAA SDM Conference, April 2004

[8] Hilburger, M. W., Nemeth, M. P., Riddick, J. C., and Thornburgh, R. P., "Effects of elastic edge restraints and initial prestress on the buckling response of compression-loaded composite panels", 45th AIAA SDM Conference, April 2004

[9] Baruch, M. and Singer, J., "Effect of eccentricity of stiffeners on the general instability of stiffened cylindrical shells under hydrostatic pressure," Journal of Mechanical Engineering Science, 5, (1) (1963) pp.23-27.

[10] Almroth, B. O. and Brogan, F. A., "The STAGS computer code", NASA CR-2950, NASA Langley Research Center, Hampton, VA, 1978.

[11] Rankin, C. C., Stehlin, P., and Brogan, F. A., "Enhancements to the STAGS computer code", NASA CR-4000, NASA Langley Research center, Hampton, VA, 1986.

[12] Riks, E., Rankin C. C., Brogan F. A., "On the solution of mode jumping phenomena in thin walled shell structures", First ASCE/ASM/SES Mechanics Conference, Charlottesville, VA, June 6-9, 1993, in: Computer Methods in Applied Mechanics and
Engineering, Vol.136, 1996.

[13] Arbocz, J., "The effect of initial imperfections on shell stability - An updated review", Delft University Faculty of Aerospace Engineering Report LR-695, September 1992.

[14] Arbocz, J. and Hol, J. M. A. M., "On the reliability of buckling load predictions", AIAA Paper 94-1371, Proc. 35th AIAA Structures, Structural Dynamics, and Materials Conference, Hilton Head SC, 514-527 (1993).

[15] Arbocz, J. and Hol, J., "Shell stability analysis in a computer aided engineering (CAE) environment", AIAA Paper 93-133, Proc. 34th AIAA Structures, Structural Dynamics, and Materials Conference, La Jolla, CA, 300-314 (1993).

[16] Stein, M, "The phenomenon of change of buckling patterns in elastic structures,", NASA Technical report R-39, NASA (1959)

[17] A. W. Leissa, "Buckling of laminated composite plates and shell panels," AFWAL-TR-85-3069, Air Force Wright Aeronautical Laboratories, Wright-Patterson AFB, Ohio 45433, June, 1985.

[18] R. R. Arnold and J. C. Parekh, "Buckling, postbuckling, and failure of flat and shallow-curved, edge-stiffened composite plates subject to combined axial compression and shear loads", Presented at 27th SDM Meeting, San Antonio, Tx., April 1986, AIAA Paper No. 86-1027-CP, 1986, Proceedings pp. 769-782.

[19] J. H. Starnes,Jr., N. F. Knight,Jr. and M. Rouse, "Postbuckling behavior of selected flat stiffened graphite-epoxy panels loaded in compression," AIAA Paper 82-0777, presented at AIAA 23rd Structures, Structural Dynamics, and Materials Conference, New Orleans, May, 1982. See also, AIAA J., 23, (8) (1985) pp.1236-1246.

[20] E. E. Spier, "On experimental versus theoretical incipient buckling of narrow graphite/epoxy plates in compression," Proc. AIAA 21st SDM Conference, AIAA Paper 80-0686-CP, May, 1980.

[21] E. E. Spier, "Local buckling, postbuckling, and crippling behavior of graphite-epoxy short thin-walled compression members," Naval Air Systems Command, Washington, D. C., NASC-N00019-80-C-0174, July 1981.

[22] N. R. Bauld, Jr. and N. S. Khot, "A numerical and experimental investigation of the buckling behavior of composite panels", Computers and Structures, 15 (1982) pp. 393-403.

[23] N. S. Khot and N. R. Bauld, Jr., "Further comparison of the numerical and experimental buckling behaviors of composite panels," Computers and Structures, 17, (1983) pp. 61-68.

[24] Y. Zhang and F. L. Matthews, "Postbuckling behavior of anisotropic laminated plates under pure shear and shear combined with compressive loading", AIAA Journal, 22, (2), (1984) pp 281-286.

[25] Stoll, F. and Gurdal, Z., "Nonlinear analysis of compressively loaded linked-plate structures," AIAA Paper 90-0968-CP, Proceedings 31st AIAA/ASME Structures, Structural Dynamics, and Materials Meeting, pp 903-913 (1990).

[26] Stoll, F. and Gurdal, Z., and Starnes, J. H., Jr., "A method for the geometrically nonlinear analysis of compressively loaded prismatic composite structures," VIPSU Center for Composite Materials and Structures Report CCMS-91-03 (VPI-E-91-01), February, 1991

[27] Shin, D. K., Gurdal, Z., and Griffin, O. H., Jr., "Minimum weight design of laminated composite plates for postbuckling performance," AIAA Paper 91-0969-CP, Proceedings 32nd AIAA/ASME Structures, Structural Dynamics, and Materials Meeting, pp 257-266 (1991)

[28] Ley, R.P., Gurdal, Z., and Johnson, E.R. (1993). Optimal design of imperfect, anisotropic, ring-stiffened cylinders under combined loads. AIAA Paper 93-1526-CP, Proceedings of 34th AIAA Structures, Structural Dynamics, and Materials Conference, Part 4, pp 1881-1889.

[29] Ley, R.P., Johnson, E.R., and Gurdal, Z. (1992). Buckling of imperfect, anisotropic, ring-stiffened cylinders under combined loads. AIAA Paper 92-2232-CP, Proceedings of 33rd AIAA Structures, Structural Dynamics, and Materials Conference, Part 1, pp 86-94.

[30] Nagendra, S., Haftka, R. T., and Gurdal, Z. (1992). Stacking sequence optimization of simply supported laminates with stability and strain constraints. AIAA Paper 92-2310-CP, Proceedings of 33rd AIAA Structures, Structural Dynamics, and Materials Conference, Part 5, pp. 2526-2535.

[31] Le Riche, R. and Haftka, R. T. (1992). Optimization of laminate stacking sequence for buckling load maximization by genetic algorithm. AIAA Paper 92-2314-CP, Proceedings of 33rd AIAA Structures, Structural Dynamics, and Materials Conference, Part 5, pp. 2564-2575.

[32] Lombardi, M., Haftka, R. T., and Cinquini, C. (1992). Optimization of composite plates for buckling by simulated annealing. AIAA Paper 92-2313-CP, Proceedings of 33rd AIAA Structures, Structural Dynamics, and Materials Conference, Part 5, pp. 2552-2563.

[33] Librescu, L. and Chang, M.-Y. (1993). Effects of geometric imperfections on vibration of compressed shear deformable laminated composite curved panels. Acta Mechanica, 96, 203-224.

[34] Librescu, L. and Souza, M. A. (1991). Postbuckling behavior of shear deformable flat panels under the complex action of thermal and in-plane mechanical loadings. AIAA Paper 91-0913-CP, Proceedings of 32rd AIAA Structures, Structural Dynamics, and Materials Conference, Part 2, pp. 917-925.

[35] Librescu, L. and Stein, M. (1991). A geometrically nonlinear theory of transversely isotropic laminated composite plates and its use in the post-buckling analysis. Thin-Walled Structdures, 11, 177-201.

[36] Graves-Smith, T.R. and Sridharan, S., "A finite strip method for the post-locally-buckled analysis of plate structures," Int. J. Mech. Sci., Vol. 20, pp 833-843 (1978)

[37] Peng, M-H and Sridharan, S., "Optimized design of stiffened panels subject to interactive buckling," AIAA Paper 90-1067-CP, Proceedings 31st AIAA/ASME Structures, Structural Dynamics, and Materials Meeting, pp 1279-1288

[38] Meyers, C. A. and Hyer, M. W. (1992). Thermally-induced, geometrically nonlinear response of symmetrically laminated composite plates. AIAA Paper 92-2539-CP, Proceedings of 33rd AIAA Structures, Structural Dynamics, and Materials Conference, Part 2, pp. 1027-1037.

[39] Nemeth, M. P. (1992). Buckling behavior of long symmetrically laminated plates subjected to compresion, shear, and inplane bending loads. AIAA Paper 92-2286-CP, Proceedings of 33rd AIAA Structures, Structural

Dynamics, and Materials Conference, Part 2, pp. 274-282.

[40] Noor, A. K., Starnes, J. H., Jr., and Peters, J. M. (1992). Thermomechanical buckling and postbuckling of multilayered composite panels. AIAA Paper 92-2541-CP, Proceedings of 33rd AIAA Structures, Structural Dynamics, and Materials Conference, Part 2, pp. 1052-1068.

[41] Bushnell, D.,"Theoretical basis of the PANDA computer program for preliminary design of stiffened panels under combined in-plane loads", Computers and Structures, v. 27, No. 4, pp 541-563 (1987).

[42] D. Bushnell, "BOSOR4: Program for stress, buckling, and vibration of complex shells of revolution," Structural Mechanics Software Series - Vol. 1, (N. Perrone and W. Pilkey, editors), University Press of Virginia, Charlottesville, 1977, pp. 11-131. See also Computers and Structures, Vol. 4, (1974) pp. 399-435; AIAA J, Vol. 9, No. 10, (1971) pp. 2004-2013; Structural Analysis Systems, Vol. 2, A. Niku-Lari, editor, Pergamon Press Oxford, 1986, pp. 25-54, and Computers and Structures, 18, (3), (1984) pp. 471-536.

[43] Vanderplaats, G. N., "ADS--a FORTRAN program for automated design synthesis, Version 2.01", Engineering Design Optimization, Inc, Santa Barbara, CA, January, 1987

[44] Vanderplaats, G. N. and Sugimoto, H., "A general-purpose optimization program for engineering design", Computers and Structures, Vol. 24, pp 13-21, 1986

[45] Koiter, W. T., "Het Schuifplooiveld by Grote Overshrijdingen van de Knikspanning", National Luchtvaart Laboratorium, The Netherlands, Report X295, November 1946 (in Dutch).

[46] STAGS Brochure (2002) available online by request: crankin@rhombuscgi.com (pdf format).

Table 1 Geometry, Material Properties, and Loading

Geometry (cylindrical shell):
- Length = 300 inches
- Radius = 100 inches
- External T-shaped major stringers
- External T-shaped major rings

Material properties (aluminum):
- Young's modulus = 10 msi
- Poisson ratio = 0.3
- Maximum allowable stress = 1.0 msi (set high to avoid active stress constraints)

Loading used for all cases:
- -100000.0 $ Axial Resultant (lb/in), Nx(1) Load Set A
- -20000.00 $ Hoop Resultant (lb/in), Ny(1) Load Set A
- 20000.00 $ In-plane shear (lb/in), Nxy(1) Load Set A
- -200.0000 $ Uniform pressure, (psi), p(1) Load Set A
- Zero loading in Load Set B

Boundary conditions:
- Simple support

Imperfection:
General buckling modal imperfection amplitude, Wimpg2 = +1.0 inch and -1.0 inch.
Imperfect shells have two load cases:
- Load Case 1: Wimpg2 = +1.0 inch
- Load Case 1: Wimpg2 = -1.0 inch

Table 2 Definitions of variables used in PANDA2 examples

Variable Number	Variable Name	Definition	Structural Part
1	B(STR)	stiffener spacing, b: STR	stringer
2	B2(STR)	width of stringer base, b2 (must be > 0)	stringer
3	H(STR)	height of stiffener (type H for sketch), h:	stringer
4	W(STR)	width of outstanding flange of stiffener, w:	stringer
5	T(1)(SKN)	thickness for layer index no.(1): SKN seg=1	panel skin
6	TSUB,substr	thickness, TSUB, of substiffener set(1):	substringer
7	HSUB,substr	height, HSUB, of substiffener set(1): SKN	substringer
8	BSUB,substr	spacing, BSUB, of substiffener set(1): SKN	substringer
9	TSUB,subrng	thickness, TSUB, of substiffener set(2):	subring
10	HSUB,subrng	height, HSUB, of substiffener set(2): SKN	subring
11	BSUB,subrng	spacing, BSUB, of substiffener set(2): SKN	subring
12	T(2)(STR)	thickness for layer index no.(2): STR seg=3	stringer web
13	T(3)(STR)	thickness for layer index no.(3): STR seg=4	stringer flange
14	B(RNG)	stiffener spacing, b: RNG	ring
15	B2(RNG)	width of ring base, b2 (zero is allowed):	ring
16	H(RNG)	height of stiffener (type H for sketch), h:	ring
17	W(RNG)	width of outstanding flange of stiffener, w:	ring
18	T(4)(RNG)	thickness for layer index no.(4):RNG seg=3	ring web
19	T(5)(RNG)	thickness for layer index no.(5):RNG seg=4	ring flange

Table 3 Starting design and optimum designs from PANDA2 with and without substiffeners (dimensions in inches)

.	.	Perfect Shell With Substiffeners	Imperfect Shell With Substiffeners	Perfect Shell Without Substiffeners	Imperfect Shell Without Substiffeners
Variable Name	Starting Design	Optimum Design	Optimum Design	Optimum Design	Optimum Design
B(STR)	20.0	14.775	11.461	5.2141	5.7718
B2(STR)	2.0	1.4775	1.1461	0.52141	0.57718
H(STR)	10.0	4.5048	4.9955	2.7194	3.8575
W(STR)	10.0	2.9341	3.5908	2.1716	2.9305
T(1)(SKN)	1.0	0.30150	0.36755	0.49158	0.55232
TSUB,substr	1.0	0.23625	0.15374	-------	-------
HSUB,substr	5.0	1.1934	0.82430	-------	-------
BSUB,substr	5.0	2.8821	2.4256	-------	-------
TSUB,subrng	1.0	0.24665	0.20833	-------	-------
HSUB,subrng	5.0	2.4665	2.0833	-------	-------
BSUB,subrng	5.0	7.0617	4.9854	-------	-------
T(2)(STR)	1.0	0.52520	0.49773	0.25874	0.33045
T(3)(STR)	1.0	0.27664	0.31908	0.17386	0.23108
B(RNG)	20.0	39.157	42.874	22.208	28.291
B2(RNG)	0.0	0.0	0.0	0.0	0.0
H(RNG)	10.0	11.046	9.5948	8.2778	8.7430
W(RNG)	10.0	4.661	8.0986	3.4935	6.2876
T(4)(RNG)	1.0	0.55228	0.95512	0.41389	0.72687
T(5)(RNG)	1.0	0.25829	0.54145	0.26031	0.43056
WEIGHT	-----	**16712 lb**	**21480 lb**	**16846 lb**	**22820 lb**

Table 4 Runstream for finding the "global" optimum design

Command	**Meaning of the command**	**Input file(s)**	**Output file(s)**
panda2log	activate PANDA2 command set	.	.
begin	user provides starting design	testax4p.BEG	testax4p.OPB
setup	PANDA2 sets up matrix templates	none	many files
decide	user chooses decision variables	testax4p.DEC	testax4p.OPD
mainsetup	user chooses loading, strategy	testax4p.OPT	none
.	.	.	.
superopt	PANDA2 finds "global" optimum	testax4p.OPT	testax4p.OPM, -.OPP
chooseplot	user chooses what to plot	testax4p.CPL	testax4p.OPL
diplot	user obtains plot hard copies	.	testax4p.5.ps, etc.
.	.	.	.
superopt	PANDA2 finds "global" optimum	testax4p.OPT	testax4p.OPM, -.OPP
chooseplot	user chooses what to plot	testax4p.CPL	testax4p.OPL
diplot	user obtains plot hard copies	.	testax4p.5.ps, etc.
.	.	.	.
superopt	PANDA2 finds "global optimum	testax4p.OPT	testax4p.OPM, -.OPP
chooseplot	user chooses what to plot	testax4p.CPL	testax4p.OPL
diplot	user obtains plot hard copies	.	testax4p.5.ps, etc.
.	.	.	.
superopt	PANDA2 finds "global optimum	testax4p.OPT	testax4p.OPM, -.OPP
chooseplot	user chooses what to plot	testax4p.CPL	testax4p.OPL
diplot	user obtains plot hard copies	.	testax4p.5.ps

Table 5 Margins computed by PANDA2 for Load Case No. 1, Subcase No. 1 for the optimized perfect shell with substiffeners (Case name = testax4p)

Mar. No.	Margin Value	Margin Definition
1	2.53E-02	Local buckling from discrete model-1.,M=2 axial halfwaves;FS=0.99
2	2.23E-01	Bending-torsion buckling; M=2 ;FS=0.999
3	3.24E-01	(m=2 lateral-torsional buckling load factor)/(FS)-1;FS=0.999
4	2.53E-02	Inter-ring bucklng, discrete model, n=6 circ.halfwaves;FS=0.999
5	4.28E+00	eff.stress:matl=1,SKN,Iseg=2,at:n=1,layer=1,z=-0.1507;-MID.;FS=1.
6	5.49E+00	matl=2 ; substiffener effective stressSTRCON MID.;FS=1.
7	1.76E+00	buckling margin stringer Iseg.3 . Local halfwaves=8 .MID.;FS=1.
8	5.68E-03	buckling margin stringer Iseg.4 . Local halfwaves=8 .MID.;FS=1.
9	7.44E-01	buckling stringer Isegs.3+4 together.M=9 ;C=0. ;MID.;FS=1.4
10	1.27E-01	buckling stringer Iseg 4 as beam on foundation. M=212;MID.;FS=3.
11	1.18E+01	buckling ring Iseg 4 as beam on foundation. M=169;MID.;FS=3.
12	1.53E-01	buck.(SAND);simp-support smearsubstf; (0.95*altsol);FS=0.999
13	-3.84E-03	buck.(SAND);simp-support inter-ring; (1.00*altsol);FS=0.999
14	-2.02E-02	buck.(SAND);simp-support general buck;M=6;N=0;slope=0.4637;FS=.999
15	2.35E-03	buck.(SAND);simp-support general buck;(0.85*altsol);FS=0.999
16	5.72E+00	buck.(SAND);rolling with smear rings; M=52;N=1;slope=0.01;FS=0.999
17	6.94E-03	buck.(SAND);rolling only of stringers;M=16;N=0;slope=0.;FS=1.6
18	1.28E+00	buck.(SAND);hiwave roll. of stringers;M=86;N=0;slope=0.;FS=1.2
19	1.73E+00	buck.(SAND); STRINGERS: web buckling;M=9;N=1;slope=0.;FS=1.
20	1.35E+01	buck.(SAND); RINGS: web buckling;M=2;N=1;slope=0.;FS=1.
21	4.60E-01	buck.(SAND);rolling with skin buckl.; M=1;N=1;slope=0.1939;FS=0.999
22	-4.04E-04	buckling:simp-support of substring.M=1;FS=1.
23	1.14E+01	buckling:simp-support of subrings N=1;FS=1.
24	-2.86E-02	buckling:simp-support altsoln4 intermajorpatch; FS=0.999
25	3.21E-01	buckling:simp-support altsoln5 skin+edgsubroll; FS=0.999
26	2.18E-01	buck.(SAND);rolling with smear substr;M=1;N=2;slope=16.67;FS=0.999
27	5.78E-02	buckling:simp-support altsoln6 inter-subring ; FS=0.999
28	5.77E+00	buck.(SAND);rolling with smear subrng;M=39;N=1;slope=0.01;FS=0.999
29	6.91E-01	buck.(SAND);rolling only of substring;M=20;N=0;slope=0.;FS=1.6
30	8.00E+00	buck.(SAND);rolling only of subrings; M=0;N=4;slope=0.;FS=1.6
31	6.43E+01	(Max.allowable ave.axial strain)/(ave.axial strain) -1; FS=1.
32	4.15E-01	1.-3.V(8)^1+V(1)^1-1 inequality constraint no. 1
33	4.59E-01	1.-3.V(11)^1+V(14)^1-1 inequality constraint no. 2
34	9.80E-01	1.+10.V(6)^1-V(7)^1-1 inequality constraint no. 3
35	0.00E+00	1.+10.V(9)^1-V(10)^1-1 inequality constraint no. 4
36	1.33E+00	1.-V(3)^1+20.V(12)^1-1 inequality constraint no. 5
37	-3.62E-05	1.-V(16)^1+20.V(18)^1-1 inequality constraint no. 6

Table 6 New margins in the case testax4p pertaining to substringers and subrings

Mar. No.	Margin Value	Margin Definition
6	5.49E+00	matl=2 ; substiffener effective stressSTRCON MID.;FS=1.
21	4.60E-01	buck.(SAND);rolling with skin buckl.; M=1;N=1;slope=0.1939;FS=0.999
22	-4.04E-04	buckling:simp-support of substring.M=1;FS=1.
23	1.14E+01	buckling:simp-support of subrings N=1;FS=1.
24	-2.86E-02	buckling:simp-support altsoln4 intermajorpatch; FS=0.999
25	3.21E-01	buckling:simp-support altsoln5 skin+edgsubroll; FS=0.999
26	2.18E-01	buck.(SAND);rolling with smear substr;M=1;N=2;slope=16.67;FS=0.999
27	5.78E-02	buckling:simp-support altsoln6 inter-subring ; FS=0.999
28	5.77E+00	buck.(SAND);rolling with smear subrng;M=39;N=1;slope=0.01;FS=0.999
29	6.91E-01	buck.(SAND);rolling only of substring;M=20;N=0;slope=0.;FS=1.6
30	8.00E+00	buck.(SAND);rolling only of subrings; M=0;N=4;slope=0.;FS=1.6

Table 7 Margins in the case testax4p for which the substiffeners are smeared out

Mar. No.	Margin Value	Margin Definition
1	2.53E-02	Local buckling from discrete model-1.,M=2 axial halfwaves;FS=0.99
2	2.23E-01	Bending-torsion buckling; M=2 ;FS=0.999
3	3.24E-01	(m=2 lateral-torsional buckling load factor)/(FS)-1;FS=0.999
4	2.53E-02	Inter-ring bucklng, discrete model, n=6 circ.halfwaves;FS=0.999
12	1.53E-01	buck.(SAND);simp-support smearsubstf; (0.95*altsol);FS=0.999
13	-3.84E-03	buck.(SAND);simp-support inter-ring; (1.00*altsol);FS=0.999
14	-2.02E-02	buck.(SAND);simp-support general buck;M=6;N=0;slope=0.4637;FS=.999
15	2.35E-03	buck.(SAND);simp-support general buck;(0.85*altsol);FS=0.999
16	5.72E+00	buck.(SAND);rolling with smear rings; M=52;N=1;slope=0.01;FS=0.999

Table 8 Optimum designs suitable for analysis with STAGS (dimensions in inches)

.	Perfect Shell With Substiffeners	Imperfect Shell With Substiffeners	Perfect Shell Without Substiffeners	Imperfect Shell Without Substiffeners
Variable Name	Optimum Design	Optimum Design	Optimum Design	Optimum Design
B(STR)	14.612	11.424	5.2360	5.7644
B2(STR)	1.4612	1.1424	0.52360	0.57644
H(STR)	4.2569	5.1430	2.6734	3.8010
W(STR)	3.1474	3.3240	2.2670	2.9990
T(1)(SKN)	0.30574	0.38290	0.48975	0.56340
TSUB,substr	0.24266	0.15810	-------	-------
HSUB,substr	1.2074	0.87730	-------	-------
BSUB,substr	2.9224	2.2848	-------	-------
TSUB,subrng	0.26422	0.20290	-------	-------
HSUB,subrng	2.6422	2.0290	-------	-------
BSUB,subrng	7.5000	4.7619	-------	-------
T(2)(STR)	0.46728	0.52520	0.25758	0.32390
T(3)(STR)	0.29086	0.29530	0.18523	0.23430
B(RNG)	37.500	42.857	21.429	27.273
B2(RNG)	0.0	0.0	0.0	0.0
H(RNG)	10.486	9.6990	9.0944	7.9770
W(RNG)	5.2204	7.7940	2.0981	6.3630
T(4)(RNG)	0.52429	0.93330	0.45472	0.72520
T(5)(RNG)	0.32008	0.50620	0.091261	0.47750
WEIGHT	16750 lb	21780 lb	17020 lb	23020 lb

Table 9 Margins for the optimized perfect shell with substiffeners. Stiffener spacings are suitable for an analysis with STAGS (Case name = testax4p, Subcase 1 only)

Mar. No.	Margin Value	Margin Definition
1	1.24E-01	Local buckling from discrete model-1.,M=2 axial halfwaves;FS=0.99
2	3.38E-01	Bending-torsion buckling; M=2 ;FS=0.999
3	4.50E-01	(m=2 lateral-torsional buckling load factor)/(FS)-1;FS=0.999
4	1.03E-02	Inter-ring bucklng, discrete model, n=6 circ.halfwaves;FS=0.999
5	4.26E+00	eff.stress:matl=1,SKN,Iseg=2,at:n=1,layer=1,z=-0.1529;-MID.;FS=1.
6	5.39E+00	matl=2 ; substiffener effective stressSTRCON MID.;FS=1.
7	1.45E+00	buckling margin stringer Iseg.3 . Local halfwaves=8 .MID.;FS=1.
8	-3.99E-03	buckling margin stringer Iseg.4 . Local halfwaves=8 .MID.;FS=1.
9	4.64E-01	buckling stringer Isegs.3+4 together.M=9 ;C=0. ;MID.;FS=1.4
10	7.63E-02	buckling stringer Iseg 4 as beam on foundation. M=198;MID.;FS=3.
11	1.43E+01	buckling ring Iseg 4 as beam on foundation. M=140;MID.;FS=3.
12	2.95E-01	buck.(SAND);simp-support smearsubstf; (0.95*altsol);FS=0.999
13	-3.76E-03	buck.(SAND);simp-support inter-ring; (1.00*altsol);FS=0.999
14	-3.66E-02	buck.(SAND);simp-support general buck;M=6;N=0;slope=0.473;FS=0.999
15	6.26E-04	buck.(SAND);simp-support general buck;(0.85*altsol);FS=0.999
16	6.26E+00	buck.(SAND);rolling with smear rings; M=50;N=1;slope=0.01;FS=0.999
17	-2.58E-02	buck.(SAND);rolling only of stringers;M=14;N=0;slope=0.;FS=1.6
18	7.89E-01	buck.(SAND);hiwave roll. of stringers;M=84;N=0;slope=0.;FS=1.2
19	1.43E+00	buck.(SAND); STRINGERS: web buckling;M=9;N=1;slope=0.;FS=1.
20	1.51E+01	buck.(SAND); RINGS: web buckling;M=2;N=1;slope=0.;FS=1.
21	4.86E-01	buck.(SAND);rolling with skin buckl.; M=1;N=1;slope=0.1978;FS=0.999
22	6.44E-03	buckling:simp-support of substring.M=1;FS=1.
23	1.41E+01	buckling:simp-support of subrings N=1;FS=1.
24	-4.18E-02	buckling:simp-support altsoln4 intermajorpatch; FS=0.999
25	3.18E-01	buckling:simp-support altsoln5 skin+edgsubroll; FS=0.999
26	1.21E-01	buck.(SAND);rolling with smear substr;M=1;N=2;slope=20.;FS=0.999
27	1.16E-02	buckling:simp-support altsoln6 inter-subring ; FS=0.999
28	6.04E+00	buck.(SAND);rolling with smear subrng;M=39;N=1;slope=0.01;FS=0.999
29	7.09E-01	buck.(SAND);rolling only of substring;M=18;N=0;slope=0.;FS=1.6
30	9.28E+00	buck.(SAND);rolling only of subrings; M=0;N=3;slope=0.;FS=1.6
31	6.33E+01	(Max.allowable ave.axial strain)/(ave.axial strain) -1; FS=1.
32	2.33E+00	0.3333 *(Stringer spacing, b)/(Stringer base width, b2)-1;FS=1.
33	1.01E+00	1.+10.V(6)^1-V(7)^1-1
34	-2.38E-07	1.+10.V(9)^1-V(10)^1-1
35	1.20E+00	1.-V(3)^1+20.V(12)^1-1
36	-1.79E-07	1.-V(16)^1+20.V(18)^1-1

Table 10 Abridged and edited version of the output file, testax4p.out2 from STAGS for a "patch" model containing three axial bays and nine circumferential bays between major stiffeners

---

threexninebays.testax4p.allshells.fasteners.480.out2 (name of STAGS case)
shift=0.98, one negative buckling mode
CONVERGENCE HAS BEEN OBTAINED FOR EIGENVALUES 1 THROUGH 8 Critical load factor

.	.	.	.	Types of buckling
NO.	Eigenvalue	Load set A	@DOF	.
1	9.773792E-01	9.773792E-01	27287	<--1st mode 4, 13, 17 (See Fig. 3)
2	9.816915E-01	9.816915E-01	17321	<--2nd mode 4, 13, 17
3	1.012336E+00	1.012336E+00	4731	<--3rd mode 1, 2, 3, 4, 13, 17
4	1.017679E+00	1.017679E+00	5335	<--4th mode 1, 2, 3, 4, 13, 17, 24
5	1.024645E+00	1.024645E+00	6877	<--5th mode 1, 2, 3, 4, 13, 17, 24
6	1.025765E+00	1.025765E+00	114463	<--6th mode 1, 2, 3, 17, 24
7	1.028083E+00	1.028083E+00	27275	<--7th mode 1, 2, 3, 17, 24
8	1.029080E+00	1.029080E+00	4605	<--8th mode 1, 2, 3, 17, 24

Table 11 Abridged and edited version of the output file, testax4p.out2 from STAGS for a model of the complete cylindrical shell with all stiffeners smeared and with use of the 480 finite element

---

entireshell.testax4p.allstiffsmeared.480.out2
shift=1.05, zero negative buckling modes
MAXIMUM NUMBER OF ITERATIONS
CONVERGENCE HAS BEEN OBTAINED FOR EIGENVALUES 1 THROUGH 5
CONVERGENCE CRITERION HAS NOT BEEN SATISFIED FOR EIGENVALUES 6 THROUGH 6

.	Critical load factor	Critical load factor	.	Types of buckling
NO.	Eigenvalue	Load set A	@DOF	.
1	1.288339E+00	1.288339E+00	12879	<--n=3 circ.waves, Fig. 9
2	1.288339E+00	1.288339E+00	12663	.
3	1.371375E+00	1.371375E+00	18375	<--n=0 circ.waves, Figs.10, 11
4	1.371375E+00	1.371375E+00	18333	.
5	1.382606E+00	1.382606E+00	12735	<--n=2 circ.waves
6	1.382625E+00	1.382625E+00	12543	<--not converged

Table 12 Margins for the optimized imperfect shell with substiffeners. Stiffener spacings are suitable for an analysis with STAGS (Case name = testax4)

Mar. No.	Margin Value	Margin Definition
1	3.51E-01	Local buckling from discrete model-1.,M=5 axial halfwaves;FS=0.99
2	1.59E-01	Long-axial-wave bending-torsion buckling; M=2 ;FS=0.999
3	2.41E-01	(m=2 lateral-torsional buckling load factor)/(FS)-1;FS=0.999
4	-2.96E-02	Ring sidesway buk., discrete model, n=7 circ.halfwaves;FS=0.999
5	8.23E-02	Hi-n Ring flang buckl.discrete model,n=52 circ.halfwaves;FS=0.999
6	5.02E+00	eff.stress:matl=1,SKN,Iseg=1,at:n=1,layer=1,z=0.1914;-MID.;FS=1.
7	6.93E+00	matl=2 ; substiffener effective stressSTRCON MID.;FS=1.
8	1.61E+00	buckling margin stringer Iseg.3 . Local halfwaves=8 .MID.;FS=1.
9	5.19E-02	buckling margin stringer Iseg.4 . Local halfwaves=8 .MID.;FS=1.
10	6.43E-01	buckling stringer Isegs.3+4 together.M=8 ;C=0. ;MID.;FS=1.4
11	2.04E-01	buckling stringer Iseg 4 as beam on foundation. M=190;MID.;FS=3.
12	2.81E+00	buckling margin ring Iseg.3 . Local halfwaves=1 .MID.;FS=1.
13	-2.37E-02	buckling ring Iseg 4 as beam on foundation. M=105;MID.;FS=3.
14	8.89E-02	buck.(SAND);simp-support smearsubstf; (0.95*altsol);FS=0.999
15	2.27E-03	buck.(SAND);simp-support inter-ring; (1.00*altsol);FS=0.999
16	-1.35E-02	buck.(SAND);simp-support general buck;M=1;N=2;slope=25.;FS=0.999
17	4.01E-02	buck.(SAND);simp-support general buck;(0.85*altsol);FS=0.999
18	6.67E+00	buck.(SAND);rolling with smear rings; M=64;N=1;slope=0.01;FS=0.999
19	1.58E-02	buck.(SAND);rolling only of stringers;M=12;N=0;slope=0.;FS=1.6
20	1.16E+00	buck.(SAND);hiwave roll. of stringers;M=75;N=0;slope=0.;FS=1.2
21	1.62E+00	buck.(SAND); STRINGERS: web buckling;M=8;N=1;slope=0.;FS=1.
22	2.98E+00	buck.(SAND); RINGS: web buckling;M=1;N=1;slope=0.2017;FS=1.
23	1.56E+00	buck.(SAND);rolling with skin buckl.; M=1;N=1;slope=0.11;FS=0.999
24	-4.82E-03	buckling:simp-support of substring.M=1;FS=1.
25	3.62E+00	buckling:simp-support of subrings N=1;FS=1.
26	-9.47E-03	buckling:simp-support altsoln4 intermajorpatch; FS=0.999
27	1.34E+00	buckling:simp-support altsoln5 skin+edgsubroll; FS=0.999
28	4.58E-01	buck.(SAND);rolling with smear substr;M=1;N=2;slope=16.67;FS=0.999
29	3.92E-01	buckling:simp-support altsoln6 inter-subring ; FS=0.999
30	8.81E+00	buck.(SAND);rolling with smear subrng;M=39;N=1;slope=0.02;FS=0.999
31	8.08E-01	buck.(SAND);rolling only of substring;M=29;N=0;slope=0.;FS=1.6
32	8.13E-01	buck.(SAND);hiwave roll. of substring;M=31;N=0;slope=0.;FS=1.6
33	1.06E-01	buck.(SAND);rolling only of subrings; M=0;N=3;slope=0.;FS=1.6
34	8.04E+01	(Max.allowable ave.axial strain)/(ave.axial strain) -1; FS=1.
35	2.33E+00	0.3333 *(Stringer spacing, b)/(Stringer base width, b2)-1;FS=1.
36	7.04E-01	1.+10.V(6)^1-V(7)^1-1
37	0.00E+00	1.+10.V(9)^1-V(10)^1-1
38	1.04E+00	1.-V(3)^1+20.V(12)^1-1
39	9.25E-01	1.-V(16)^1+20.V(18)^1-1

Table 13 Margins for the optimized imperfect shell with substiffeners. Stiffener spacings are suitable for an analysis with STAGS. The design is the same as that for Table 12 but the amplitude of the initial imperfection has been set equal to zero.

Mar. No.	Margin Value	Margin Definition
1	3.31E-01	Local buckling from discrete model-1.,M=5 axial halfwaves;FS=0.99
2	2.21E-01	Long-axial-wave bending-torsion buckling; M=2 ;FS=0.999
3	3.14E-01	(m=2 lateral-torsional buckling load factor)/(FS)-1;FS=0.999
4	5.34E-01	Inter-ring bucklng, discrete model, n=8 circ.halfwaves;FS=0.999
5	5.63E+00	eff.stress:matl=1,SKN,Iseg=2,at:n=1,layer=1,z=-0.1914;-MID.;FS=1.
6	7.11E+00	matl=2 ; substiffener effective stressSTRCON MID.;FS=1.
7	1.72E+00	buckling margin stringer Iseg.3 . Local halfwaves=8 .MID.;FS=1.
8	1.35E-01	buckling margin stringer Iseg.4 . Local halfwaves=8 .MID.;FS=1.
9	7.26E-01	buckling stringer Isegs.3+4 together.M=8 ;C=0. ;MID.;FS=1.4
10	2.99E-01	buckling stringer Iseg 4 as beam on foundation. M=190;MID.;FS=3.
11	2.54E+01	buckling ring Iseg 4 as beam on foundation. M=105;MID.;FS=3.
12	2.71E-01	buck.(SAND);simp-support smearsubstf; (0.95*altsol);FS=0.999
13	7.45E-02	buck.(SAND);simp-support inter-ring; (1.00*altsol);FS=0.999
14	1.96E-01	buck.(SAND);simp-support general buck;M=1;N=2;slope=25.;FS=0.999
15	4.78E-01	buck.(SAND);simp-support general buck;(0.85*altsol);FS=0.999
16	6.90E+00	buck.(SAND);rolling with smear rings; M=64;N=1;slope=0.01;FS=0.999
17	7.94E-02	buck.(SAND);rolling only of stringers;M=12;N=0;slope=0.;FS=1.6
18	1.29E+00	buck.(SAND);hiwave roll. of stringers;M=75;N=0;slope=0.;FS=1.2
19	1.71E+00	buck.(SAND); STRINGERS: web buckling;M=8;N=1;slope=0.;FS=1.
20	7.05E+01	buck.(SAND); RINGS: web buckling;M=1;N=1;slope=0.;FS=1.
21	2.99E+00	buck.(SAND);rolling with skin buckl.; M=1;N=1;slope=0.1756;FS=0.999
22	3.87E-02	buckling:simp-support of substring.M=1;FS=1.
23	1.82E+01	buckling:simp-support of subrings N=1;FS=1.
24	1.94E-01	buckling:simp-support altsoln4 intermajorpatch; FS=0.999
25	2.69E+00	buckling:simp-support altsoln5 skin+edgsubroll; FS=0.999
26	6.03E-01	buck.(SAND);rolling with smear substr;M=1;N=1;slope=14.29;FS=0.999
27	5.63E-01	buckling:simp-support altsoln6 inter-subring ; FS=0.999
28	1.02E+01	buck.(SAND);rolling with smear subrng;M=43;N=1;slope=0.02;FS=0.999
29	7.72E-01	buck.(SAND);rolling only of substring;M=29;N=0;slope=0.;FS=1.6
30	7.77E-01	buck.(SAND);hiwave roll. of substring;M=31;N=0;slope=0.;FS=1.6
31	1.16E+01	buck.(SAND);rolling only of subrings; M=0;N=3;slope=0.;FS=1.6
32	8.04E+01	(Max.allowable ave.axial strain)/(ave.axial strain) -1; FS=1.
33	2.33E+00	0.3333 *(Stringer spacing, b)/(Stringer base width, b2)-1;FS=1.
34	7.04E-01	1.+10.V(6)^1-V(7)^1-1
35	0.00E+00	1.+10.V(9)^1-V(10)^1-1
36	1.04E+00	1.-V(3)^1+20.V(12)^1-1
37	9.25E-01	1.-V(16)^1+20.V(18)^1-1

Table 14 Margins for Load case 1, Subcase 1 for the perfect optimized externally T-stiffened cylindrical shell without substiffeners for the optimum design suitable for analysis by STAGS (case name = testax3)

Mar. No.	Margin Value	Margin Definition
1	2.12E-01	Local buckling from discrete model-1.,M=1 axial halfwaves;FS=0.99
2	2.37E-01	Bending-torsion buckling; M=1 ;FS=0.999
3	5.73E+00	eff.stress:matl=1,STR,Dseg=5,node=11,layer=1,z=0.2449; MID.;FS=1.
4	3.07E-01	(m=1 lateral-torsional buckling load factor)/(FS)-1;FS=0.999
5	1.57E-01	Inter-ring bucklng, discrete model, n=32 circ.halfwaves;FS=0.999
6	5.73E+00	eff.stress:matl=1,SKN,Iseg=1,at:n=1,layer=1,z=0.2449;-MID.;FS=1.
7	1.27E+00	buckling margin stringer Iseg.3 . Local halfwaves=8 .MID.;FS=1.
8	4.52E-02	buckling margin stringer Iseg.4 . Local halfwaves=8 .MID.;FS=1.
9	2.65E-01	buckling stringer Isegs.3+4 together.M=7 ;C=0. ;MID.;FS=1.4
10	1.48E-01	buckling stringer Iseg 4 as beam on foundation. M=292;MID.;FS=3.
11	3.53E-01	buck.(SAND);simp-support local buck.; (0.95*altsol);FS=0.999
12	2.58E-03	buck.(SAND);simp-support inter-ring; (1.00*altsol);FS=0.999
13	-3.53E-02	buck.(SAND);simp-support general buck;M=8;N=0;slope=0.335;FS=0.999
14	1.52E-01	buck.(SAND);simp-support general buck;(0.85*altsol);FS=0.999
15	1.28E+01	buck.(SAND);rolling with smear rings; M=152;N=1;slope=0.01;FS=0.999
16	5.13E-02	buck.(SAND);rolling only of stringers;M=18;N=0;slope=0.;FS=1.6
17	4.74E-01	buck.(SAND);hiwave roll. of stringers;M=123;N=0;slope=0.;FS=1.2
18	5.32E+01	buck.(SAND);rolling only axisym.rings;M=0;N=0;slope=0.;FS=1.6
19	1.27E+00	buck.(SAND); STRINGERS: web buckling;M=8;N=1;slope=0.;FS=1.
20	7.73E+03	buck.(SAND); RINGS: web buckling;M=1;N=8;slope=0.;FS=1.
21	7.37E+01	(Max.allowable ave.axial strain)/(ave.axial strain) -1; FS=1.
22	2.33E+00	0.3333 *(Stringer spacing, b)/(Stringer base width, b2)-1;FS=1.
23	9.27E-01	1.-V(3)^1+20.V(6)^1-1
24	-5.96E-08	1.-V(10)^1+20.V(12)^1-1

Table 15 Margins for Load case 1, Subcase 1 for the imperfect optimized externally T-stiffened cylindrical shell without substiffeners for the optimum design suitable for analysis by STAGS (case name = testax3)

Mar. No.	Margin Value	Margin Definition
1	3.73E-01	Local buckling from discrete model-1.,M=1 axial halfwaves;FS=0.99
2	3.75E-01	Bending-torsion buckling; M=1 ;FS=0.999
3	6.72E+00	eff.stress:matl=1,STR,Dseg=5,node=11,layer=1,z=0.2812; MID.;FS=1.
4	3.54E-01	(m=1 lateral-torsional buckling load factor)/(FS)-1;FS=0.999
5	4.74E-01	Ring flang buckling,discrete model,n=51 circ.halfwaves;FS=0.999
6	5.10E-02	Lo-n Ring sidesway, discrete model, n=8 circ.halfwaves;FS=0.999
7	6.39E+00	eff.stress:matl=1,RNG,Iseg=3,at:TIP,layer=1,z=0.3626;-MID.;FS=1.
8	1.09E+00	buckling margin stringer Iseg.3 . Local halfwaves=7 .MID.;FS=1.
9	7.63E-03	buckling margin stringer Iseg.4 . Local halfwaves=7 .MID.;FS=1.
10	2.06E-01	buckling stringer Isegs.3+4 together.M=7 ;C=0. ;MID.;FS=1.4
11	1.80E-01	buckling stringer Iseg 4 as beam on foundation. M=221;MID.;FS=3.
12	3.00E+00	buckling margin ring Iseg.3 . Local halfwaves=1 .MID.;FS=1.
13	6.61E-02	buckling ring Iseg 4 as beam on foundation. M=114;MID.;FS=3.
14	8.69E-01	buck.(SAND);simp-support local buck.; (0.95*altsol);FS=0.999
15	1.03E-01	buck.(SAND);simp-support inter-ring; (1.00*altsol);FS=0.999
16	3.15E-02	buck.(SAND);simp-support general buck;M=1;N=3;slope=3.4427;FS=0.999
17	3.86E-03	buck.(SAND);simp-support general buck;(0.85*altsol);FS=0.999
18	1.75E+01	buck.(SAND);rolling with smear rings; M=110;N=1;slope=0.01;FS=0.999
19	-4.77E-03	buck.(SAND);rolling only of stringers;M=12;N=0;slope=0.;FS=1.6
20	4.47E-01	buck.(SAND);hiwave roll. of stringers;M=92;N=0;slope=0.;FS=1.2
21	1.03E+00	buck.(SAND); STRINGERS: web buckling;M=7;N=1;slope=0.;FS=1.
22	3.27E+00	buck.(SAND); RINGS: web buckling;M=1;N=1;slope=0.1864;FS=1.
23	9.45E+01	(Max.allowable ave.axial strain)/(ave.axial strain) -1; FS=1.
24	2.33E+00	0.3333 *(Stringer spacing, b)/(Stringer base width, b2)-1;FS=1.
25	7.04E-01	1.-V(3)^1+20.V(6)^1-1
26	8.18E-01	1.-V(10)^1+20.V(12)^1-1

Table 16 Margins for Load case 2, Subcase 1 for the imperfect optimized externally T-stiffened cylindrical shell without substiffeners for the optimum design suitable for analysis by STAGS (case name = testax3)

Mar. No.	Margin Value	Margin Definition
1	2.59E-02	Local buckling from discrete model-1.,M=1 axial halfwaves;FS=0.99
2	2.77E-02	Bending-torsion buckling; M=1 ;FS=0.999
3	6.85E+00	eff.stress:matl=1,SKN,Dseg=2,node=6,layer=1,z=0.2812; MID.;FS=1.
4	8.51E-02	(m=1 lateral-torsional buckling load factor)/(FS)-1;FS=0.999
5	5.46E-02	Inter-ring bucklng, discrete model, n=37 circ.halfwaves;FS=0.999
6	6.39E+00	eff.stress:matl=1,RNG,Iseg=3,at:TIP,layer=1,z=0.3626;-MID.;FS=1.
7	1.56E+00	buckling margin stringer Iseg.3 . Local halfwaves=7 .MID.;FS=1.
8	3.71E-01	buckling margin stringer Iseg.4 . Local halfwaves=7 .MID.;FS=1.
9	5.53E-01	buckling stringer Isegs.3+4 together.M=7 ;C=0. ;MID.;FS=1.4
10	6.06E-01	buckling stringer Iseg 4 as beam on foundation. M=221;MID.;FS=3.
11	3.00E+00	buckling margin ring Iseg.3 . Local halfwaves=1 .MID.;FS=1.
12	6.61E-02	buckling ring Iseg 4 as beam on foundation. M=114;MID.;FS=3.
13	4.09E-02	buck.(SAND);simp-support local buck.; (0.95*altsol);FS=0.999
14	2.69E-02	buck.(SAND);simp-support inter-ring; (1.00*altsol);FS=0.999
15	3.15E-02	buck.(SAND);simp-support general buck;M=1;N=3;slope=3.443;FS=0.999
16	7.52E-02	buck.(SAND);simp-support general buck;(0.85*altsol);FS=0.999
17	7.39E-01	buck.(SAND);rolling with smear string;M=1;N=14;slope=33.33;FS=0.999
18	1.68E+01	buck.(SAND);rolling with smear rings; M=112;N=1;slope=0.01;FS=0.999
19	3.10E-01	buck.(SAND);rolling only of stringers;M=12;N=0;slope=0.;FS=1.6
20	9.10E-01	buck.(SAND);hiwave roll. of stringers;M=92;N=0;slope=0.;FS=1.2
21	9.09E-02	buck.(SAND);rolling only of rings; M=0;N=8;slope=0.;FS=1.6
22	6.24E-01	buck.(SAND);hiwave roll. of rings; M=0;N=45;slope=0.;FS=1.2
23	1.32E+00	buck.(SAND); STRINGERS: web buckling;M=7;N=1;slope=0.;FS=1.
24	3.27E+00	buck.(SAND); RINGS: web buckling;M=1;N=1;slope=0.1864;FS=1.
25	9.45E+01	(Max.allowable ave.axial strain)/(ave.axial strain) -1; FS=1.

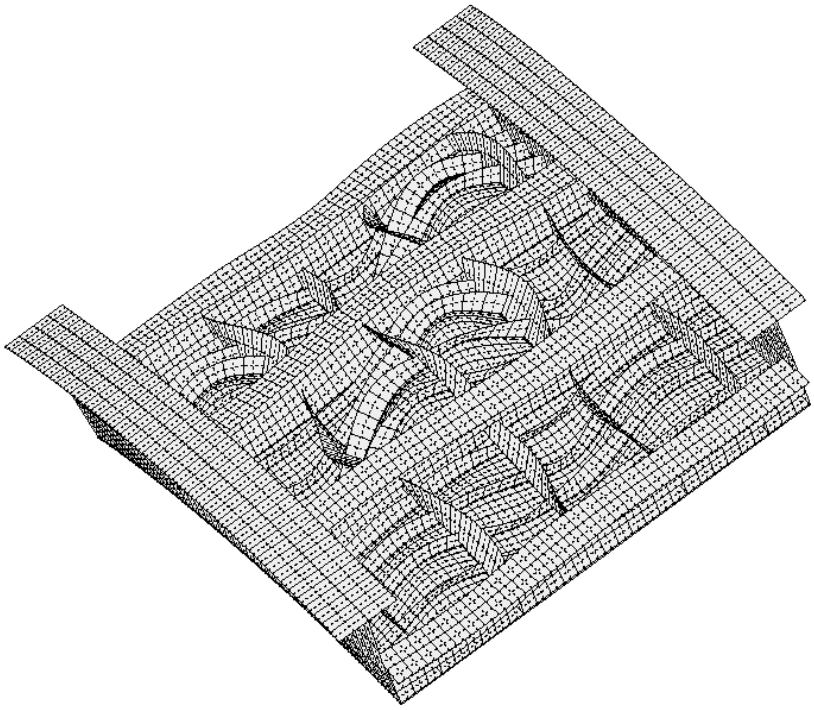

Fig. 1 STAGS model interring testax4p.allshells.1x3bays, mode 1, Pcr = .98903

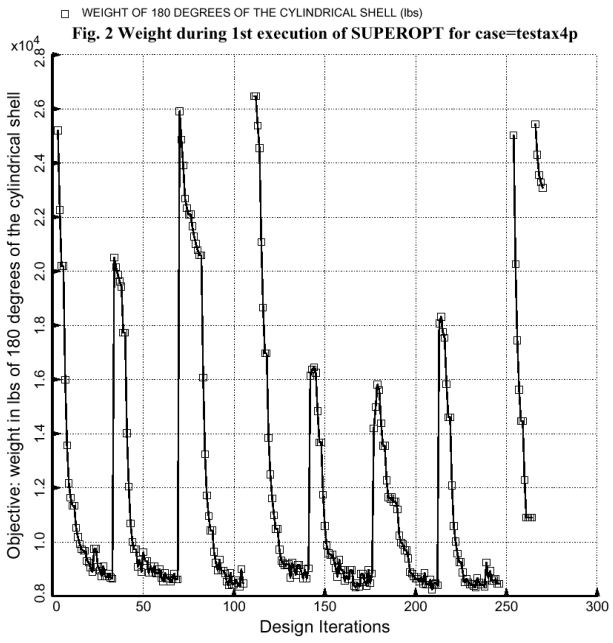

Fig. 2 Weight during 1st execution of SUPEROPT for case=testax4p

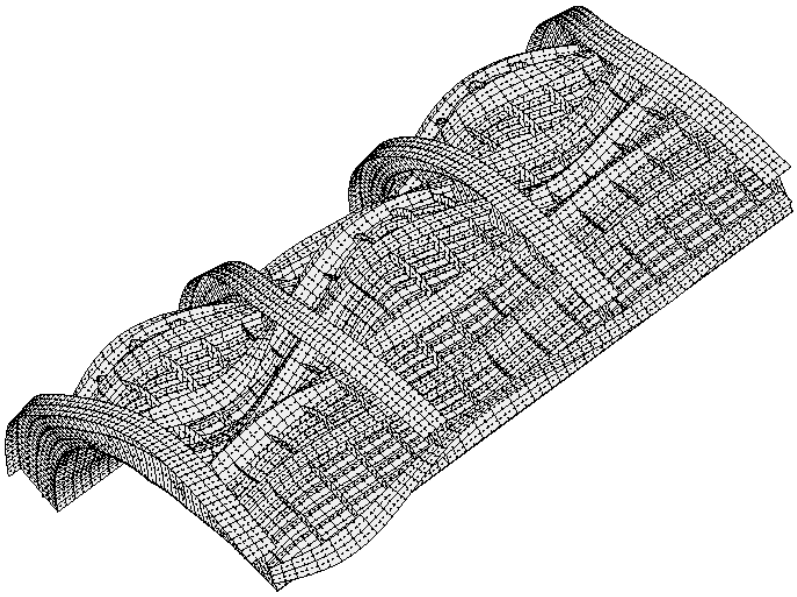

Fig. 3 STAGS model, threexninebays.testax4p.allshells.fasteners, mode 1, Pcr = .97738

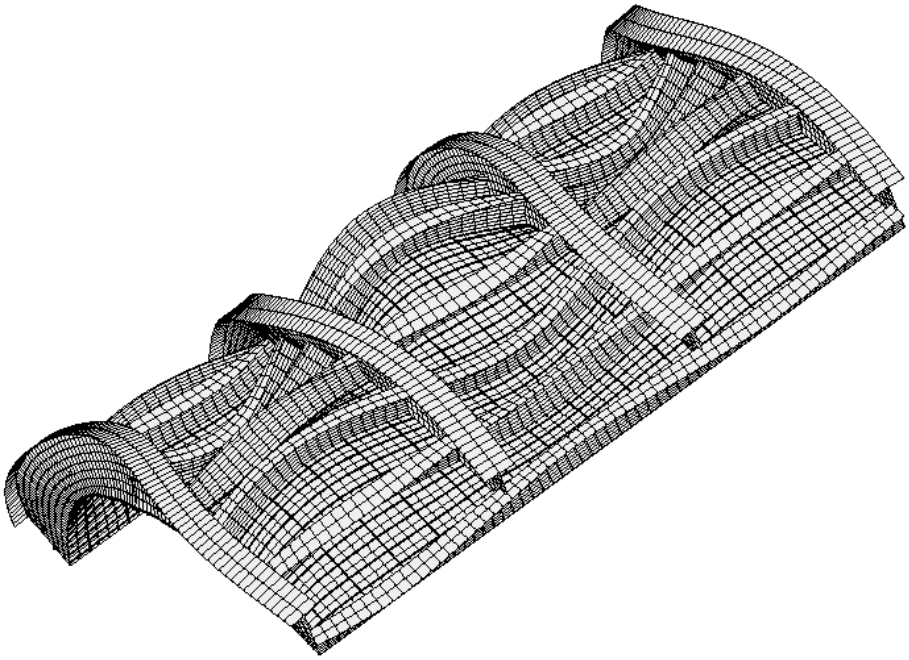

Fig. 4 STAGS model, threexninebay.testax4p.substiffbeams.majorstiffshells.410, mode 1, Pcr = 1.0259

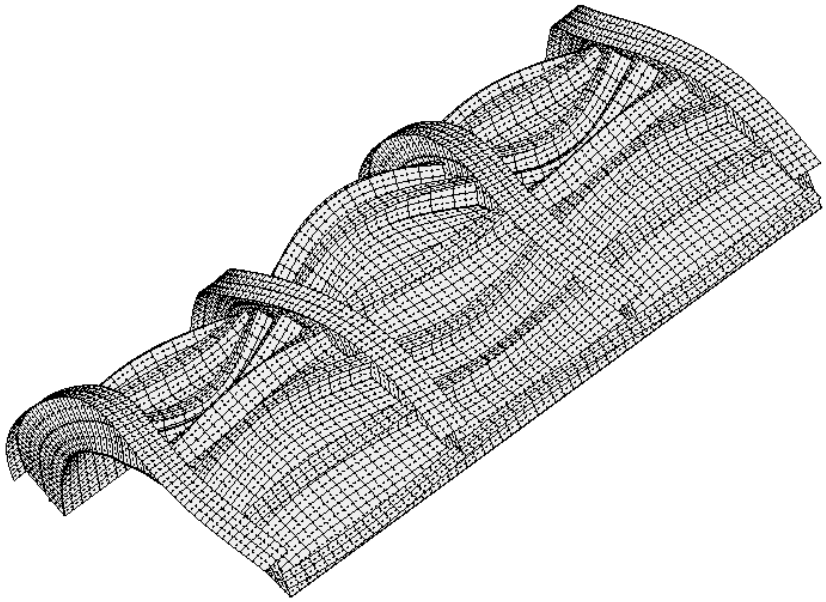

Fig. 5 STAGS model, threexninebay.testax4p.substiffsmeared.majorstiffshells.480, mode 1, Pcr = .98903

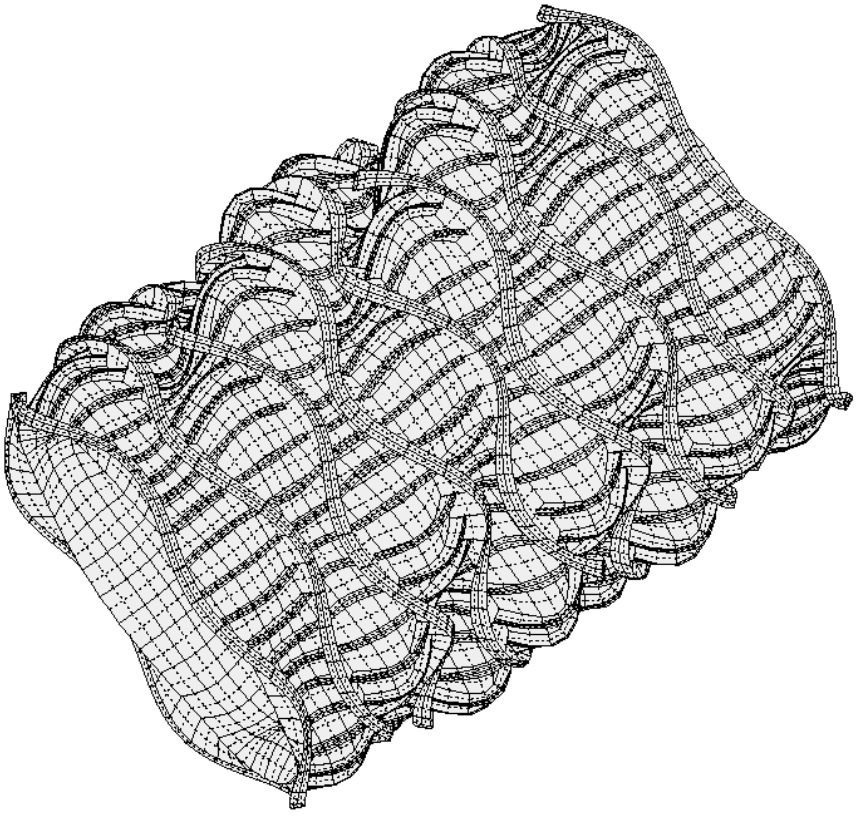

Fig. 6 STAGS model, entireshell.testax4p.substiffsmeared.majorstiffshells.480, mode 1, Pcr = 1.0222

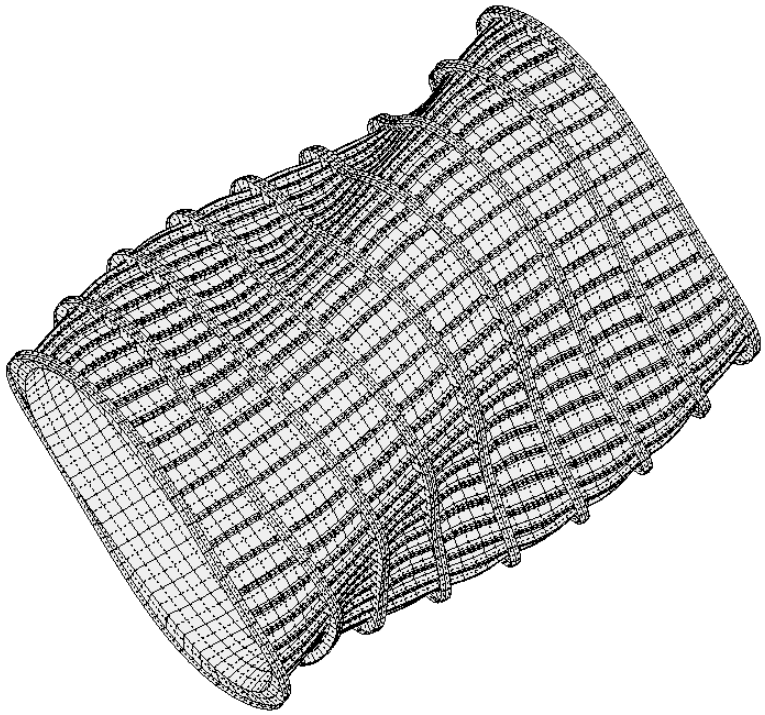

Fig. 7 STAGS model, entireshell.testax4p.substiffsmeared.majorstiffshells.480, mode 19, Pcr = 1.0511

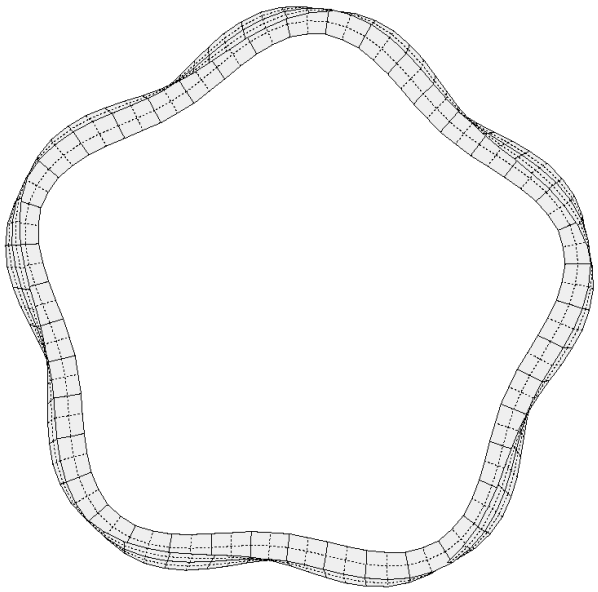

Fig. 8 STAGS model, fourth ring, entireshell.testax4p.substiffsmeared.majorstiffshells.480

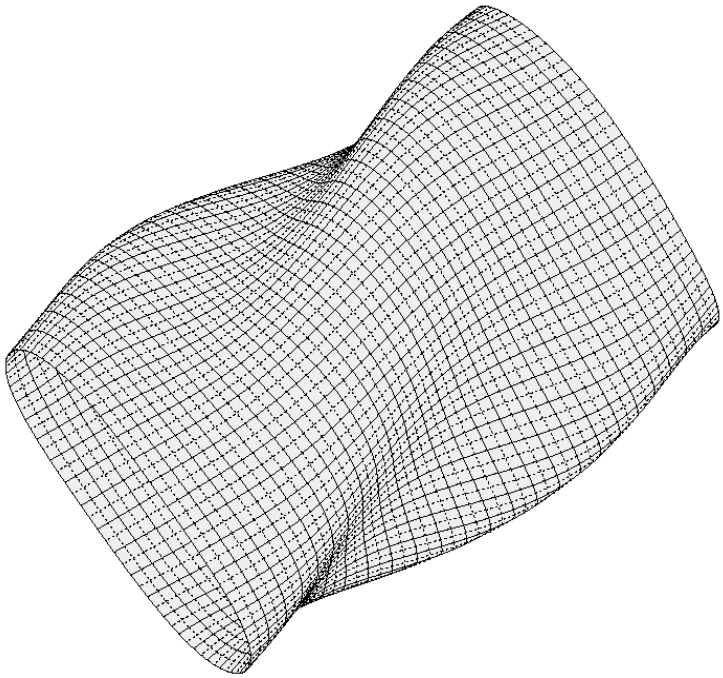

Fig. 9 STAGS model, entireshell.testax4p.allstiffsmeared.480, mode 1, Pc = 1.2883

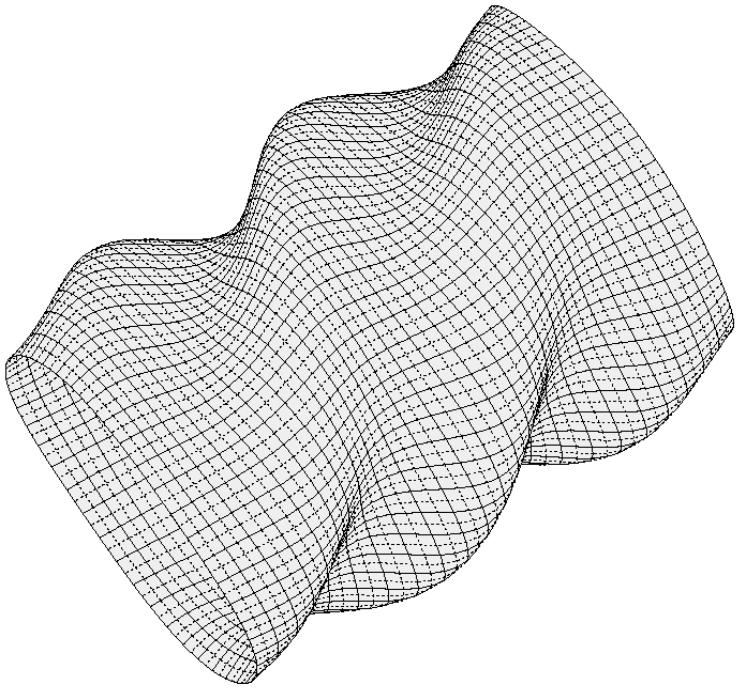

Fig. 10 STAGS model, entireshell.testax4p.allstiffsmeared.480, mode 3, Pc = 1.3714

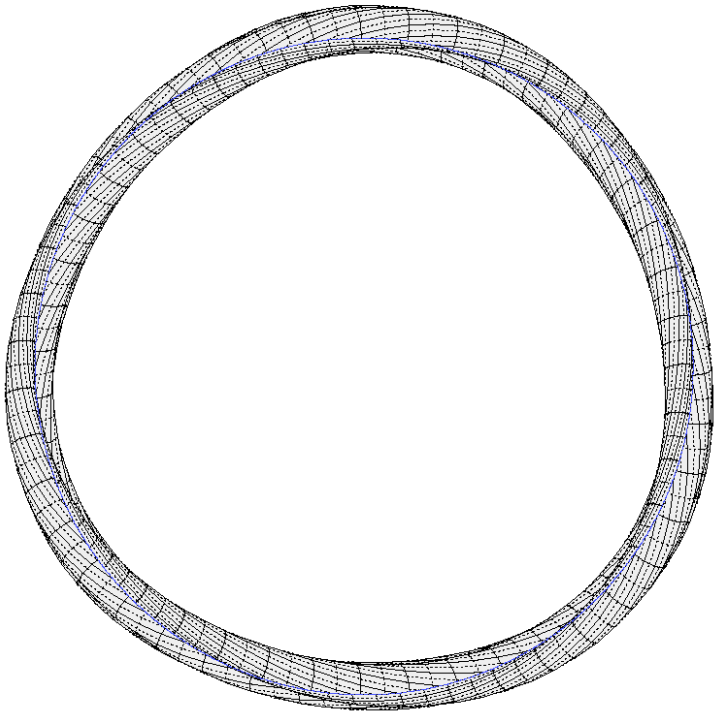

Fig. 11, End view of model in Fig. 10

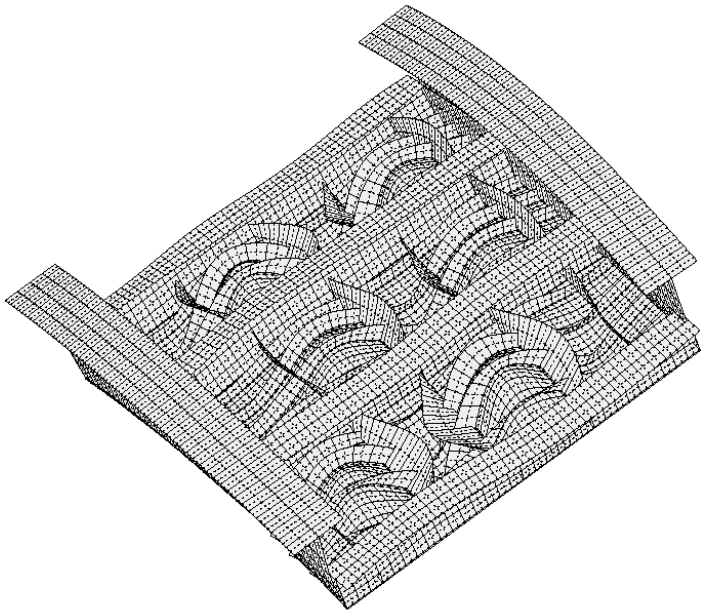

Fig. 12 STAGS model, interring.testax4p.allshells.1x3bays.fasteners.480, mode 4, Pcr = 1.0278

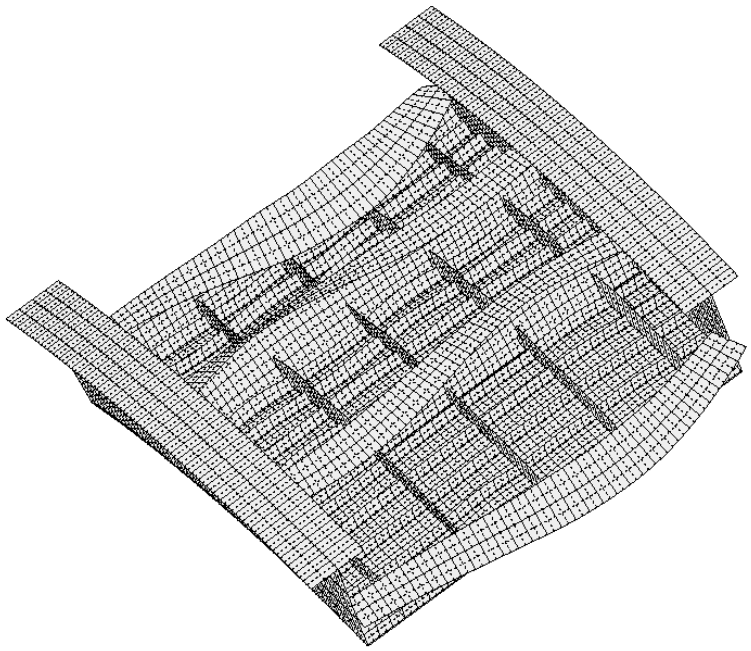

Fig. 13 STAGS model, interring.testax4p.allshells.1x3bays.fasteners.480 mode 16, Pcr = 1.1668

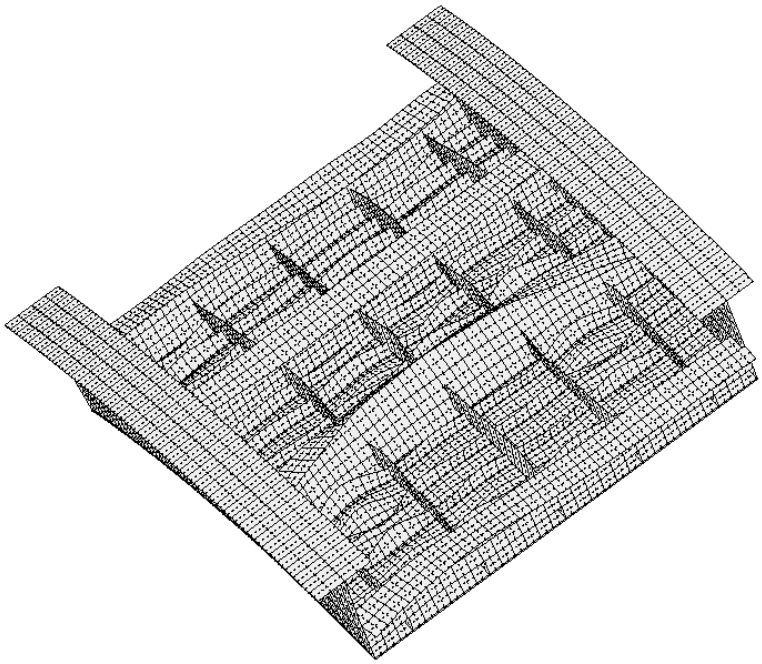

Fig. 14 STAGS model, interring.testax4p.allshells.1x3bays.fasteners.480 mode 34, Pcr = 1.3113

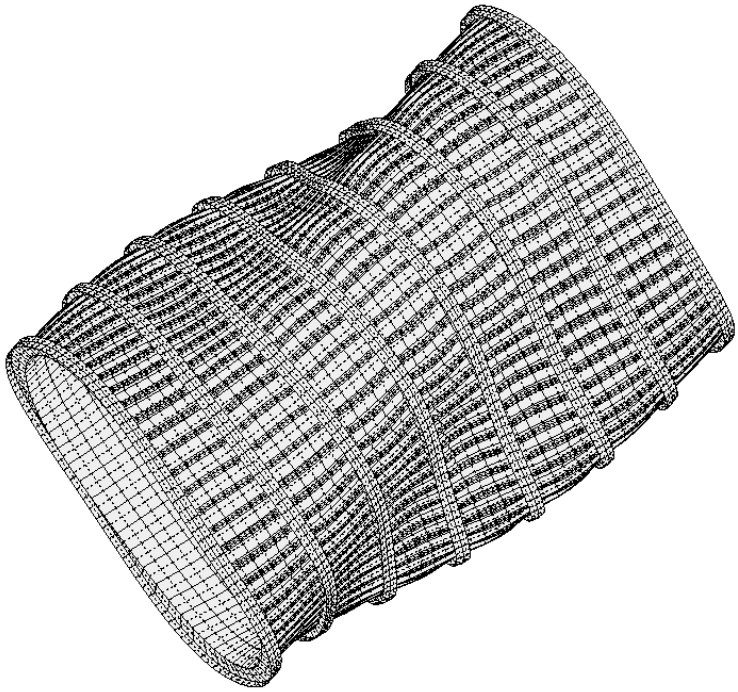

Fig. 15 STAGS model, entireshell.testax4.substiffsmeared.majorstiffshells.480, mode1, Pcr = 1.4468

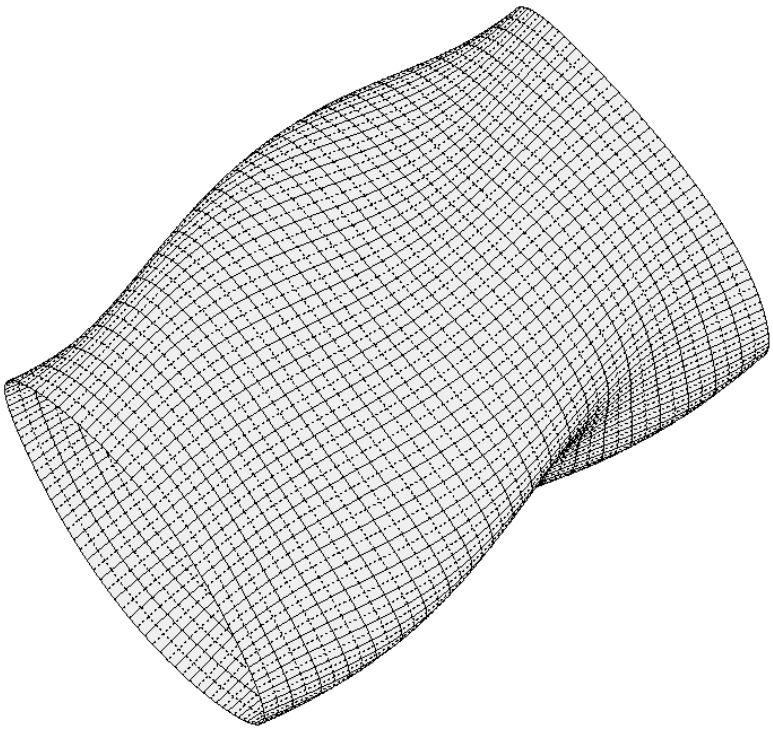

Fig. 16 STAGS model, entireshell.testax4.allstiffsmeared.480, mode 1, Pcr = 1.8058

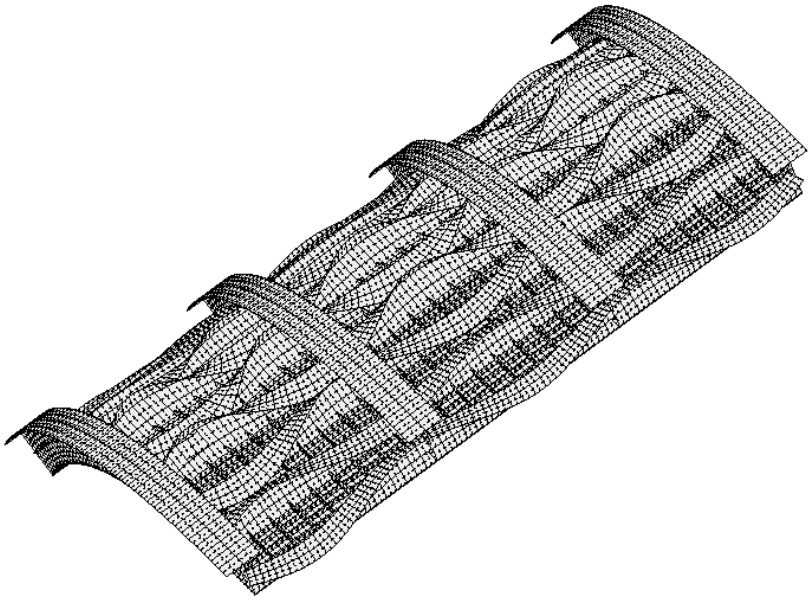

Fig. 17 STAGS model, threexninebays.testax4.allshells.fasteners.480, mode 2 Pcr = 1.2557

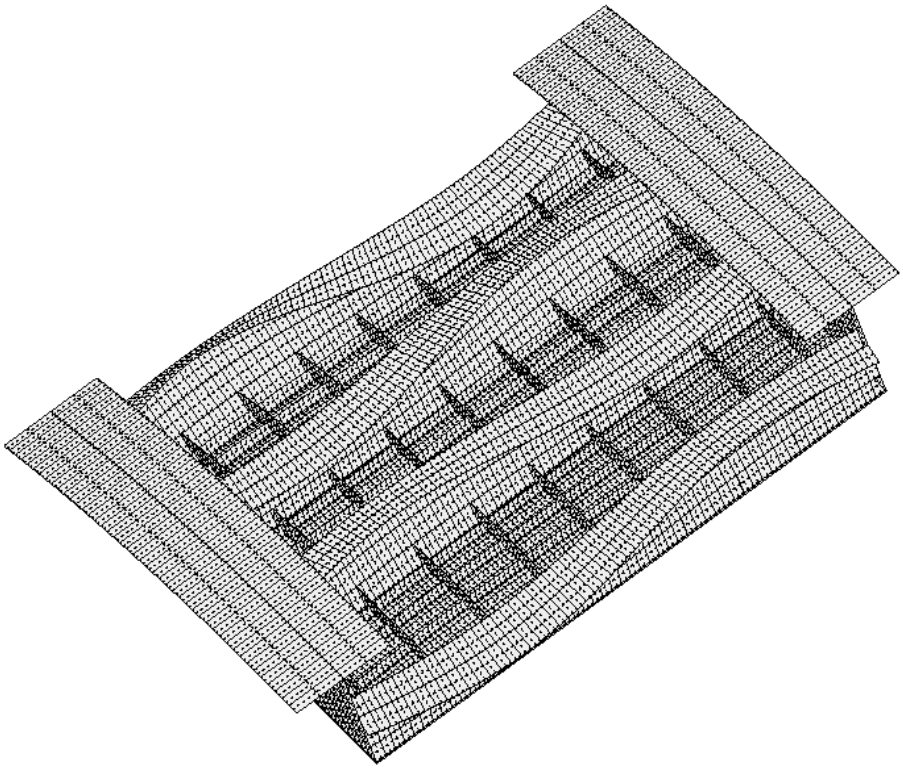

Fig. 18 STAGS model, interring.testax4.allshells.1x3bays.fasteners.480, mode 1, Pcr = 1.2757

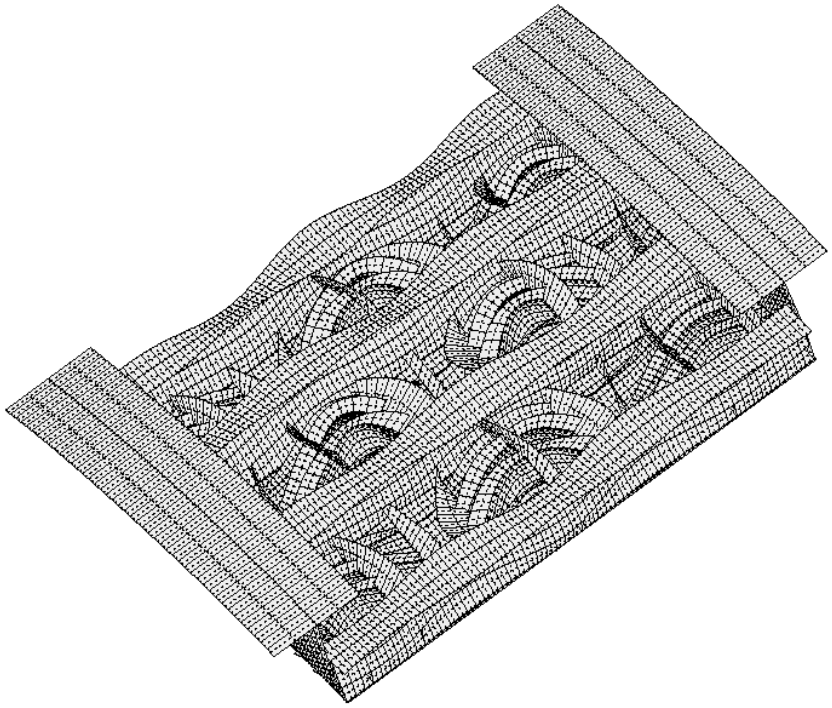

Fig. 19 STAGS model, interring.testax4.allshells.1x3bays.fasteners.480, mode 3, Pcr = 1.3099

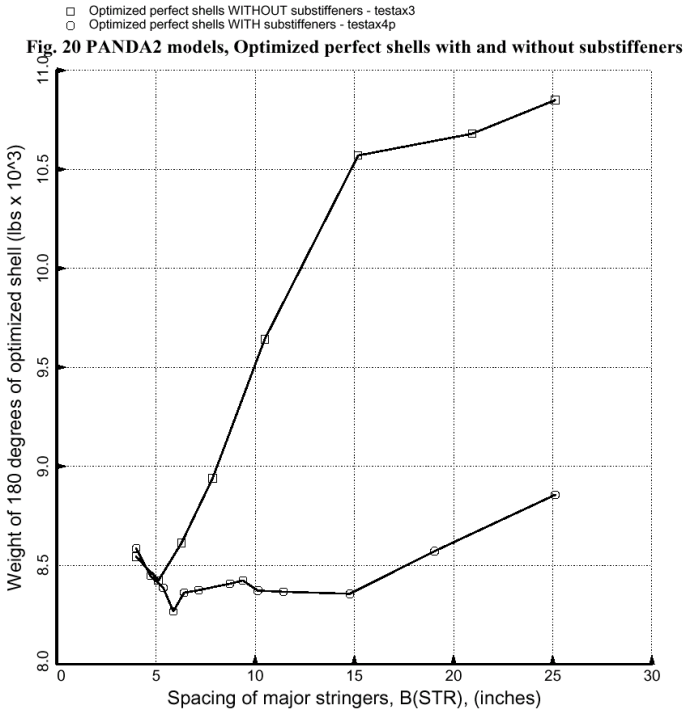

Fig. 20 PANDA2 models, optimized perfect shells with and without substiffeners

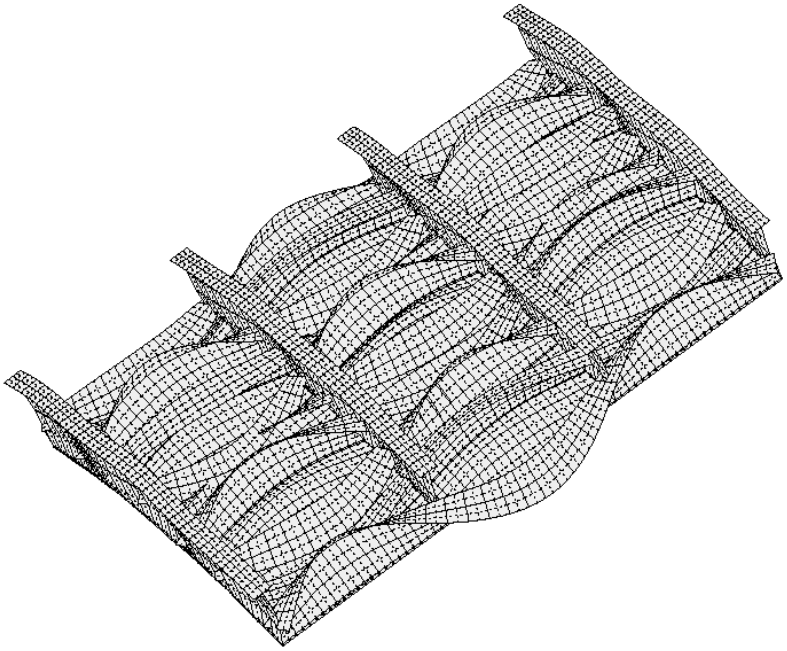

Fig 21 STAGS model, threexninebays.testax3.allshells.fasteners.480, mode 1, Pcr = 1.0042

Fig 22, STAGS model, threexninebays.testax3.allshells.fasteners.480.perfect, mode 1, Pcr = 1.0042

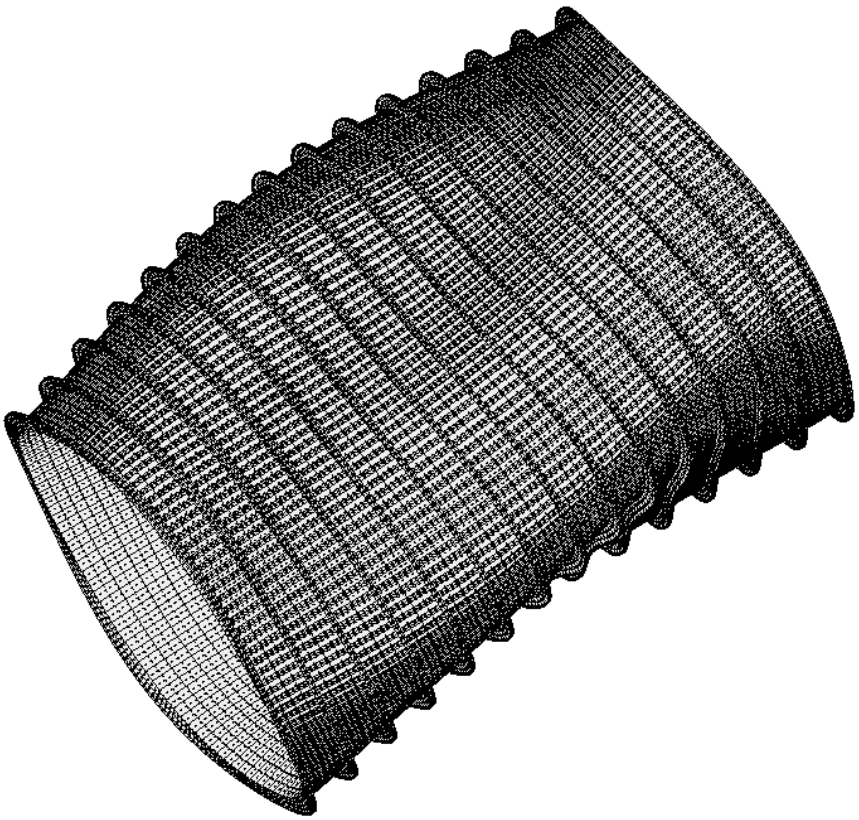

Fig. 23 STAGS model, testax3.perfect.allshells.480, mode 25, Pcr = 1.0606

Fig. 24 STAGS model, testax3.perfect.allshells.480, mode 1, Pcr = 1.0512